



University of Dundee

Low Cell Number Proteomic Analysis Using In-Cell Protease Digests Reveals a Robust Signature for Cell Cycle State Classification

Kelly, Van; Al-Rawi, Aymen; Lewis, David; Kustatscher, Georg; Ly, Tony

Published in:
Molecular & Cellular Proteomics

DOI:
[10.1016/j.mcpro.2021.100169](https://doi.org/10.1016/j.mcpro.2021.100169)

Publication date:
2022

Licence:
CC BY

Document Version
Publisher's PDF, also known as Version of record

[Link to publication in Discovery Research Portal](#)

Citation for published version (APA):

Kelly, V., Al-Rawi, A., Lewis, D., Kustatscher, G., & Ly, T. (2022). Low Cell Number Proteomic Analysis Using In-Cell Protease Digests Reveals a Robust Signature for Cell Cycle State Classification. *Molecular & Cellular Proteomics*, 21(1), Article 100169. <https://doi.org/10.1016/j.mcpro.2021.100169>

General rights

Copyright and moral rights for the publications made accessible in Discovery Research Portal are retained by the authors and/or other copyright owners and it is a condition of accessing publications that users recognise and abide by the legal requirements associated with these rights.

Take down policy

If you believe that this document breaches copyright please contact us providing details, and we will remove access to the work immediately and investigate your claim.

Low Cell Number Proteomic Analysis Using In-Cell Protease Digests Reveals a Robust Signature for Cell Cycle State Classification

Authors

Van Kelly, Aymen al-Rawi, David Lewis, Georg Kustatscher, and Tony Ly

Correspondence

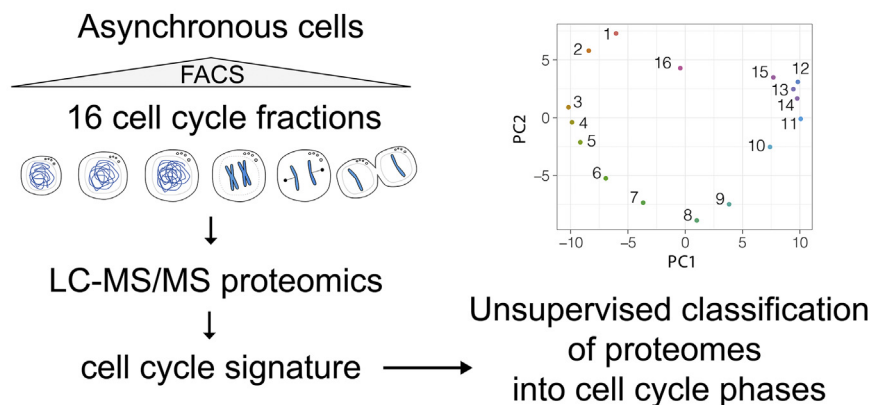
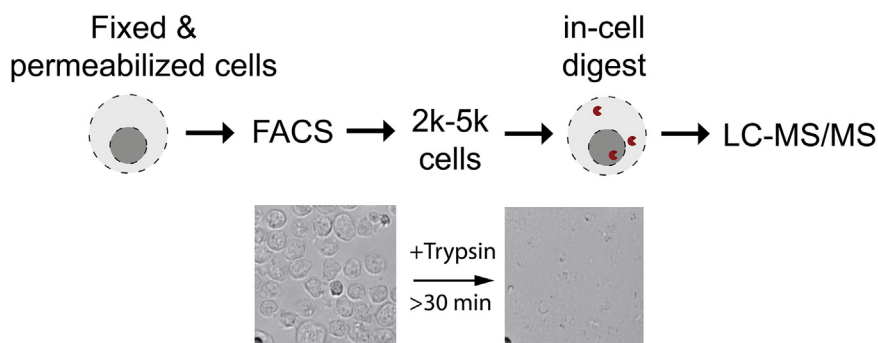
tly@ed.ac.uk

In Brief

We introduce a streamlined sample processing method for bottom-up proteomics called the “in-cell digest.” Fixed cells are directly digested by trypsin to peptides for LC-MS/MS. Combined with AMPL, we analyze the proteomes of 16 unperturbed cell cycle populations using 2500 cells for each. We identify a 119-protein cell cycle signature. Using this signature, we show unbiased classification of proteomes in proteomeHD into specific cell cycle phases. Precise cell cycle classification will be important in dissecting single-cell proteome heterogeneity.

Graphical Abstract

Low cell number proteomics using the **in-cell digest**



Highlights

- The in-cell digest is a minimalistic sample processing method for proteomics.
- Fixed cells are directly digested by trypsin into peptides for LC-MS/MS.
- Quantitative proteomes for 16 cell cycle populations (2500 cells each).
- A cell cycle signature classifies proteomes in proteomeHD into cell cycle phases.
- Peptide analysis using the Orbitrap Elite is improved by using AMPL.

Low Cell Number Proteomic Analysis Using In-Cell Protease Digests Reveals a Robust Signature for Cell Cycle State Classification

Van Kelly^{1,2}, Aymen al-Rawi¹, David Lewis¹, Georg Kustatscher² , and Tony Ly^{1,3,*} 

Comprehensive proteome analysis of rare cell phenotypes remains a significant challenge. We report a method for low cell number MS-based proteomics using protease digestion of mildly formaldehyde-fixed cells in cellulose, which we call the “in-cell digest.” We combined this with averaged MS1 precursor library matching to quantitatively characterize proteomes from low cell numbers of human lymphoblasts. About 4500 proteins were detected from 2000 cells, and 2500 proteins were quantitated from 200 lymphoblasts. The ease of sample processing and high sensitivity makes this method exceptionally suited for the proteomic analysis of rare cell states, including immune cell subsets and cell cycle subphases. To demonstrate the method, we characterized the proteome changes across 16 cell cycle states (CCSs) isolated from an asynchronous TK6 cells, avoiding synchronization. States included late mitotic cells present at extremely low frequency. We identified 119 pseudoperiodic proteins that vary across the cell cycle. Clustering of the pseudoperiodic proteins showed abundance patterns consistent with “waves” of protein degradation in late S, at the G2&M border, midmitosis, and at mitotic exit. These clusters were distinguished by significant differences in predicted nuclear localization and interaction with the anaphase-promoting complex/cyclosome. The dataset also identifies putative anaphase-promoting complex/cyclosome substrates in mitosis and the temporal order in which they are targeted for degradation. We demonstrate that a protein signature made of these 119 high-confidence cell cycle-regulated proteins can be used to perform unbiased classification of proteomes into CCSs. We applied this signature to 296 proteomes that encompass a range of quantitation methods, cell types, and experimental conditions. The analysis confidently assigns a CCS for 49 proteomes, including correct classification for proteomes from synchronized cells. We anticipate that

this robust cell cycle protein signature will be crucial for classifying cell states in single-cell proteomes.

The proteome is a functional readout of cellular phenotype, which includes dynamic and persistent features that reflect cell state and cell type, respectively. Rare cell phenotypes play key physiological roles. Quiescent stem cells, while often rare relative to differentiated cell types in a tissue, are essential for tissue homeostasis. Similarly, mitosis is a dynamic cell state that is critical for the accurate propagation of genetic information. Mitotic states are generally short lived and thus rare in an asynchronous population. Proteomic analysis of these critically important cell phenotypes is a major challenge because typical proteomic workflows require $>10^5$ cells as input.

We previously developed an approach called “PRIMMUS” or “PRoteomics of Intracellular IMMUnostained cell Subsets” to analyze abundant and rare cell cycle states (CCSs) (1). Formaldehyde-fixed cells are fractionated into specific cell states by staining cells for intracellular markers and separating them using fluorescence-activated cell sorting (FACS). Cells grown in asynchronous culture are immediately fixed, thereby minimizing perturbation to physiological processes. This step is critical, as small molecule-based synchronization can lead to effects on the proteome that are associated with stress responses arising from arrest rather than cell cycle regulation *per se* (2). PRIMMUS enabled analysis of interphase and mitotic subpopulations, but this approach was limited to relatively abundant subpopulations for which $>10^5$ cells can be collected by FACS within a reasonable time (3).

Low input proteome analysis requires specialized methods for handling low cell number of cells (4, 5). Major improvements have been made by adapting methods used for bulk samples to low cell number samples (6–8). Recent advances in small volume sample handling to nanoliter volumes have

From the ¹Wellcome Centre for Cell Biology, School of Biological Sciences, and ²Institute of Quantitative Biology, Biochemistry and Biotechnology, University of Edinburgh, Edinburgh, UK; ³Centre for Gene Regulation and Expression, School of Life Sciences, University of Dundee, Dundee, UK

*For correspondence: Tony Ly, tly@ed.ac.uk.

also enabled analysis of <10 cultured human cells, with overall number of proteins detected scaling with cell number (4, 9, 10). For example, ~3000 proteins were identified from ten HeLa cells using “nanodroplet processing in one pot for trace samples” (nanoPOTS) (11). In general, these methods have specialized requirements, ranging from automated robotic sample handling to custom microfabricated chips, which are challenging to satisfy in most laboratories currently.

Cells fixed with formaldehyde introduce additional challenges for bottom-up MS-based proteomics. Formaldehyde crosslinks proteins by forming methylene bridges primarily between lysine residues. Peptide/protein crosslinks are broken with heating to >65 °C. As an example, formalin-fixed tissue processing protocols include heating for 1 h at 95 °C. However, the fixative concentration and treatment duration for formalin-fixed tissues is much higher (4% formaldehyde for up to several hours). Studies on synthetic peptides demonstrated that protein amino acid residues can be irreversibly modified by formaldehyde, producing chemical modifications and corresponding mass shifts that are not included in conventional database searches (12, 13). In contrast, formaldehyde fixation for immune cell immunostaining and flow cytometry in clinical and academic research settings is frequently much lower (0.1–3%) and carried out under controlled conditions with limited treatment duration (10–30 min).

Here, we report a methodological advance that eliminates several steps previously required for processing fixed cells for proteomics. We demonstrate that fixed cells in suspension can be directly digested by trypsin without heat-induced crosslink reversal for quantitative proteomics. We call this streamlined approach the *in-cell digest*. The *in-cell digest* provides major improvements in sensitivity and convenience in performing proteomic analysis on low numbers of fixed cells. To overcome the duty cycle limitations of the Orbitrap Elite instrument, we developed an acquisition method called averaged MS1 precursor library matching (AMPL). We applied the *in-cell digest* and AMPL with PRIMMUS to analyze the proteomic variation during an unperturbed cell cycle in human lymphoblasts with unparalleled temporal resolution to produce unbiased proteomic definitions of CCS.

EXPERIMENTAL PROCEDURES

Experimental Design and Statistical Rationale

Four biological replicates of 16 cell cycle populations were collected by FACS, with two technical replicates of the 64 samples being acquired by LC-MS (AMP acquisition strategy) resulting in 128 LC-MS analyses, providing eight pseudotimecourses for periodicity analysis. Three libraries were generated from 12 high pH reversed-phase (HPRP) fractions of unsorted cells, interphase cells, and mitotic cells. Each library fraction was analyzed twice (or thrice for the mitotic library) resulting in a library of 85 LC-MS analyses. Libraries

were used to increase proteome coverage through MS1 feature matching.

Supporting experiments include the analysis of 12 HPRP fractions of formaldehyde fixed, fixed and reversed, and nonfixed control without replicates for a qualitative comparison of peptide modifications. About 12 cell titration samples were also collected in duplicate up to 2000 cells by FACS, including a zero-cell control, to assess LC-MS sensitivity of the improved processing and AMP acquisition methods. The 24 cell titration samples were analyzed by AMP LC-MS along with a 12 HPRP fraction library and an unfractionated library of 2000 sorted cells, which were analyzed by data-dependent acquisition (DDA) LC-MS. To assess the impact of peptide filtering on MS1 feature matching false discovery rate (FDR), unmodified, dimethylated, and isopropylated peptides were analyzed by AMPL and DDA, along with a library of 12 HPRP fractions.

Cell Culture

TK6 human lymphoblasts (14) were obtained from the Earnshaw laboratory (University of Edinburgh). Cells were cultured at 37 °C in the presence of 5% CO₂ as a suspension in RPMI1640 + GlutaMAX (Thermo Fisher Scientific) supplemented with 10% v/v fetal bovine serum (Thermo Fisher Scientific). Cell cultures were maintained at densities no higher than 2×10^6 cells per ml. MCF10A cells (American Type Culture Collection) were cultured in phenol red-free F12/Dulbecco's modified Eagle's medium (Thermo Fisher Scientific) supplemented with 5% horse serum, 10 µg/ml insulin (Sigma), 100 ng/ml cholera toxin (Sigma), 20 ng/ml epidermal growth factor (Sigma), 0.5 µg/ml hydrocortisone (Sigma), 100 units/ml penicillin, and 100 µg/ml streptomycin (Thermo Fisher Scientific) at 37 °C in the presence of 5% CO₂. Cells were maintained at less than 100% confluency and discarded when passage number exceed 20 passages. U2OS cells (American Type Culture Collection) were cultured in Dulbecco's modified Eagle's medium high glucose + GlutaMAX (Thermo Scientific) supplemented with 10% v/v fetal bovine serum (Thermo Fisher Scientific). Cells were checked for mycoplasma at the point of cryo-storage using a luminescence-based assay (Lonza).

Cell Fixation and Immunostaining

Cells were washed with Dulbecco's PBS (DPBS; Lonza) and resuspended in freshly prepared 1% formaldehyde solution (w/v) from a 16% stock (w/v; Thermo Fisher Scientific) in DPBS, fixed for 10 min at room temperature with gentle rotation, pelleted, washed with DPBS, and permeabilized with cold 90% methanol. Cells were stored at -20 °C prior to staining.

Cells stored in methanol were washed with DPBS and resuspended in blocking buffer, which is composed of 5% bovine serum albumin (BSA) in 0.1 M Tris-buffered saline, pH 7.4. Cells were blocked for 10 min at room temperature, pelleted, and resuspended in primary antibody solution. The rat anti-H3S28ph HTA28 (abcam; ab10543), mouse anticyclin A2 (Cell Signaling Technologies; 4656S), and rabbit anticyclin B1 (12231S) were used for staining as 1:200 dilutions in blocking buffer. Cells were stained with primary antibody overnight at 4 °C. Stained cells were then washed twice with wash buffer (DPBS + 0.5% BSA) and stained with dye-conjugated secondary antibodies. The donkey antirat IgG H&L AlexaFluor 568 preadsorbed (abcam; ab175475), donkey antimouse IgG (H + L) highly cross adsorbed secondary antibody, Alexa Fluor 488 (Thermo; A21202), and goat anti-rabbit IgG H&L (Alexa Fluor 647) preadsorbed (abcam; ab150083) were used as 1:200 dilutions in blocking buffer. Cells were stained for 1 h at room temperature, washed twice with DPBS, pelleted, and stained in 4',6-diamidino-2-phenylindole solution (Sigma; 20 µg/ml in DPBS + 0.1% BSA) for at least 1 h prior to FACS.

FACS and Gating Strategy

Cells were collected using a BD FACSAria Fusion Cell Sorter equipped with 355 nm UV, 405 nm violet, 488 nm blue, 561 nm YG and 640 nm red lasers, and controlled by BD FACS Diva V8.0.1 software. Cells were first gated into “narrow” (P1–P8) and “wide” (P9–P16) populations based on 4',6-diamidino-2-phenylindole fluorescence signal width. The narrow population contains single cells either in interphase or in mitosis up to late anaphase. These single cells were then separated based on cyclin B into eight different stages of interphase. Population P1 has low to no cyclin B protein and 2 N DNA content, consistent with low to no E2F activity and a G0/early G1 cell state. Cyclin B rises monotonically from P2 to P6 and then rises more steeply from P6 to P8. Like cyclin B, cyclin A also increases during interphase, but at a faster rate from P1 to P6 as compared with P6 to P8. P9 to P13 are positive for histone H3 phosphorylation at Ser28 (pH3+). Highest levels of pH3+ are present in prometaphase and metaphase. Rising and declining H3 phosphorylation in early and late mitosis, respectively, result in low to medium levels of pH3+. Cyclin A and cyclin B levels are used to further discriminate mitotic subphases, as they are degraded during prometaphase and the metaphase-to-anaphase transition, respectively.

Finally, late mitotic subphases are enriched in the wide population, but so too are doublets. We reasoned that most doublets will have cyclin B signal, as single cells with the exception of P1 are cyclin B positive. Thus, we can further enrich late mitotic stages by selecting wide, 4N, cyclin B negative cells (P14–P16). P14 to P16 are then discriminated further by pH3+ levels, which decrease during mitotic exit. We note that P16 may contain doublets of G0/early G1 cells (P1), but P14 and P15 should not as P14 and P15 are pH3+, and G0/early G1 cells are negative for pH3.

About 5000 cells for each gated population were collected using four-way purity using either an 85 or 100 μm nozzle, into 1.5 ml Eppendorf Protein Lo-Bind tubes. Four biological replicates were collected. An interphase library sample was collected by combining 300,000 cells of G0/G1, S, and G2 populations. A mitotic library sample was composed of 800,000 mitotic cells gated by high DNA content and high histone H3 Ser28 phosphorylation. Samples were centrifuged, and supernatant was removed before storing at $-20\text{ }^{\circ}\text{C}$.

In-Cell Digest

Cell-sorted library samples, and unstained unsorted TK6 cells, were resuspended in DPBS at 2 to 5 million cells per ml and incubated with 1 μl (25–29 U) benzonase (Millipore) at 37 $^{\circ}\text{C}$ for a minimum of 1 h. Trypsin was added to approximately 1:25 w/w, and in-cell digested at 37 $^{\circ}\text{C}$ for ~16 h. Digests were acidified with TFA and desalted over Sep-Pak C18 cartridges (Waters) and dried.

Individual populations of 5000 cells were diluted with 40 μl PBS and incubated with 0.25 μl (6–7 U) benzonase at 37 $^{\circ}\text{C}$ for a minimum of 1 h, then digested with 50 ng trypsin (~1:10 w/w) at 37 $^{\circ}\text{C}$ for ~16 h. Samples were acidified with TFA and desalted over self-made C18 columns with three Empore C18 disks and eluted directly into Axygen 96-well PCR Microplates (Thermo Fisher Scientific) and dried.

HPRP Fractionation

Approximately 100 μg interphase, mitotic, and unsorted TK6 cell digests were fractionated by HPRP chromatography using an Ultimate 3000 HPLC (Thermo Fisher Scientific) and a 1 \times 100 mm 1.7 μm Acquity UPLC BEH C18 column (Waters). Peptides were separated using a constant 10 mM ammonium formate (pH 10) and a gradient of water and 100% acetonitrile. Peptides were loaded at 1%

acetonitrile followed by separation by a 48 min multistep gradient of acetonitrile from 3% to 6%, 25%, 45%, and 80% acetonitrile at 4, 34, 44, and 45 min, respectively, followed by an 80% wash and re-equilibration. Fractions were collected at 30 s intervals resulting in 96 fractions, which were concatenated into 12, and 1 μg aliquots dried.

LC-MS/MS

Peptide samples were resuspended in 0.1% TFA. Approximately 0.5 μg of library fractions were injected for DDA LC-MS analysis. A volume equal to half the cell population (equivalent to ~2500 cells) was injected and analyzed twice by AMPL to produce two technical replicates for each of the four biological replicates. An Ultimate 3000 RSLCnano HPLC (Dionex, Thermo Fisher Scientific) was coupled *via* electrospray ionization to an Orbitrap Elite Hybrid Ion Trap-Orbitrap (Thermo Fisher Scientific). Peptides were loaded directly onto a 75 $\mu\text{m} \times 50\text{ cm}$ PepMap-C18 EASY-Spray LC Column (Thermo Fisher Scientific) and eluted at 250 nl/min using 0.1% formic acid (solvent A) and 80% acetonitrile/0.1% formic acid (solvent B). Samples were eluted over 90 min stepped linear gradient from 1% to 30% B over 72 min, then to 45% B over 18 min. AMPL analyses included up to five MS1 microscans of 1E6 ions in the Orbitrap at a resolution of 120 K and with a 250 ms maximum injection time. MS1 scans were acquired over 350 to 1700 m/z , and a “lock mass” of 445.120025 m/z was used. This was followed by five data-dependent MS2 collision-induced dissociation events (5E3 target ion accumulation) in the ion trap at rapid resolution with a 2 Da isolation width, a normalized collision energy of 35, 50 ms maximum fill time, a requirement of a 10 K precursor intensity, and a charge of 2+ or more. Precursors within 5 ppm were dynamically excluded for 40 s. DDA analyses were as for AMPL but with a single MS1 microscan with a 75 ms maximum injection time, followed by 20 CID events in the ion trap.

Libraries were acquired as for DDA analyses or acquired with ten data-dependent MS2 higher energy collision dissociation events at 30 normalized collision energy of 5E4 ions in the Orbitrap at 15 K resolution and a maximum fill time of 100 ms, with a precursor intensity required to be at least 50 K. For the sample preparation comparisons, a 240 min gradient was used (1%–30% B for 210 min, then to 42% B over 30 min). MS data were acquired as for DDA analysis described previously with the exception that MS1 spectra were acquired at 60 K resolution, and MS2 events were acquired only on 2+ and 3+ precursors.

MS/MS Data Analysis

Data were processed using MaxQuant, version 1.6.2.6 (15). LC-MS/MS data were searched against the Human Reference Proteome from UniProt including splice isoforms (accessed October 23, 2017), which contains 93,613 entries, allowing for two tryptic missed cleavages, allowing for variable methionine oxidation and protein N-terminal acetylation. Carbamidomethyl cysteine modification was allowed only for samples that were alkylated by iodoacetamide. The parameter “Individual peptide mass tolerance” was selected for variable precursor mass tolerances, with 0.5 Da or 20 ppm mass tolerances set for ion trap or orbitrap fragment ions, respectively. A target-decoy threshold of 1% was set for both peptide-spectrum match and protein FDR. Match-between-runs (MBR) was enabled with identification transfer within 0.5 min and a retention time alignment within 20 min window. Matching was permitted from the library parameter group and “from and to” the unfractionated parameter group. The parameter “Require MS/MS for label-free quantitation comparisons” was deselected, and second peptide search was enabled. Both modified and unmodified unique and razor peptides were used for

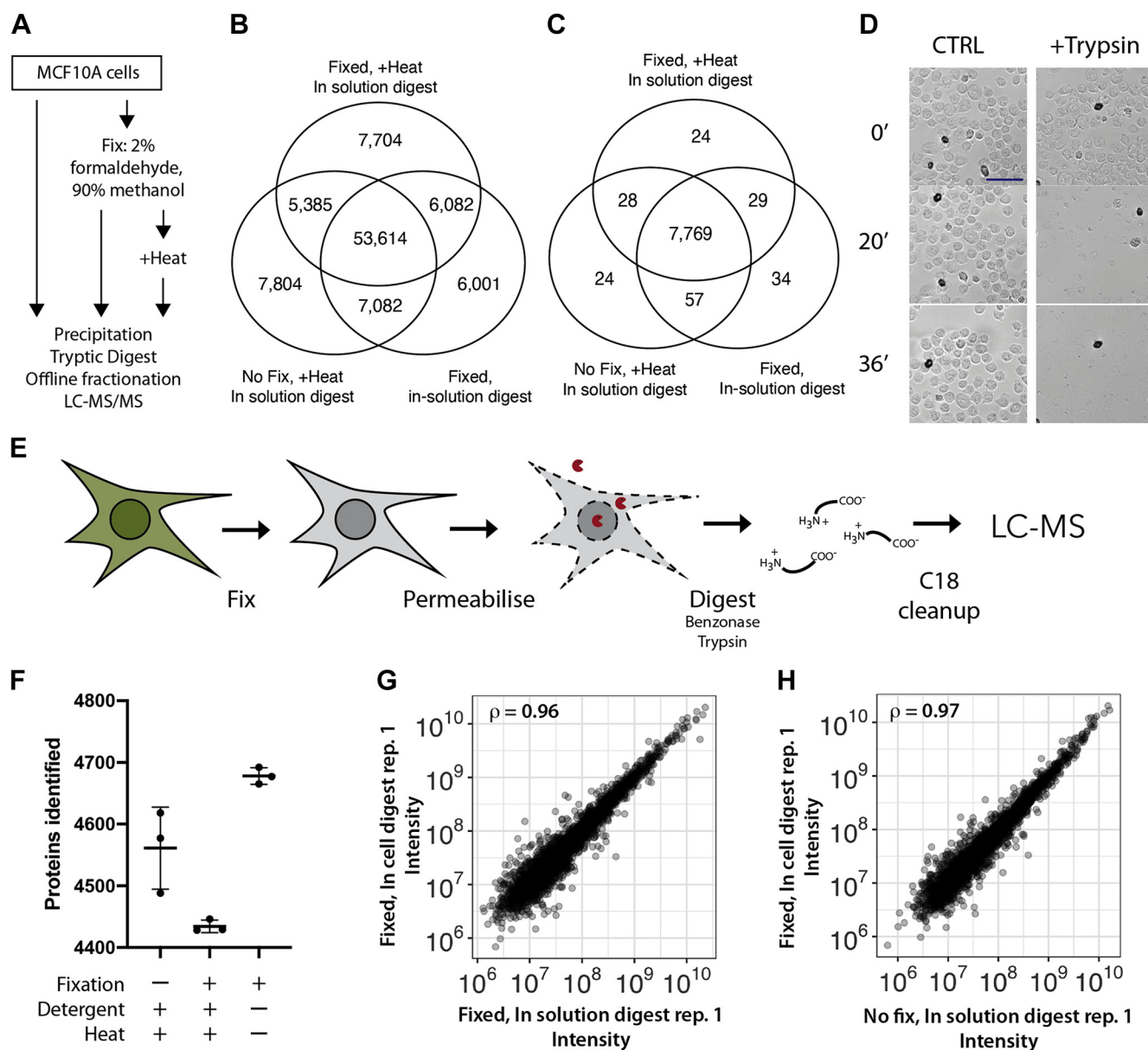


FIG. 1. A simplified workflow for proteomics of formaldehyde-fixed cells using in-cell digestion. *A*, proteomics workflow to assess impact of formaldehyde-induced modifications on proteome analysis. *B* and *C*, the number of peptides (*B*) and proteins (*C*) identified. *D*, fixed and permeabilized cells treated either with DPBS (*left*) or with trypsin (*right*) were imaged at the indicated times in minutes. The scale bar represents 50 μm . *E*, schematic of the in-cell digest workflow. *F–H*, comparison of the identification (*F*) and quantitative reproducibility (*G* and *H*) between in-solution and in-cell digests. DPBS, Dulbecco's PBS.

quantification. Protein groups with fewer than two peptides were discarded for the subsequent analysis.

MBR FDR Filtering

A reference sample was generated by lysing TK6 cells in DPBS with 2% SDS and cCOMPLETE protease inhibitors without EDTA (Roche; 1 \times concentration) at 70 $^{\circ}\text{C}$, homogenized with a probe sonicator, and treated with benzonase. Protein was reduced with 20 mM Tris(2-carboxyethyl)phosphine for 2 h before alkylation with 20 mM iodoacetamide at ambient temperature in the dark for 1 h. Protein was precipitated with four volumes of cold acetone at -20°C

overnight and washed with 100% cold acetone and 90% cold ethanol. Protein pellet was air dried before resuspending in DPBS and digesting with 1:50 w/w trypsin for ~ 16 h. Peptides were acidified, desalted, aliquoted, and fractionated as previously described. For isopropylation, 50 μg peptides were resuspended in 200 μl 90% acetonitrile containing 0.1% formic acid before addition of 50 μl acetone containing 36 $\mu\text{g}/\mu\text{l}$ NaBH_3CN . The reaction was conducted at ambient temperature for ~ 16 h before quenching with ammonium bicarbonate, drying off solvent, and desalting peptides over C18. For dimethylation, 50 μg peptide was resuspended in 200 μl DPBS before addition of 0.32% formaldehyde and 50 mM NaBH_3CN . The reaction was conducted at ambient temperature for ~ 16 h before

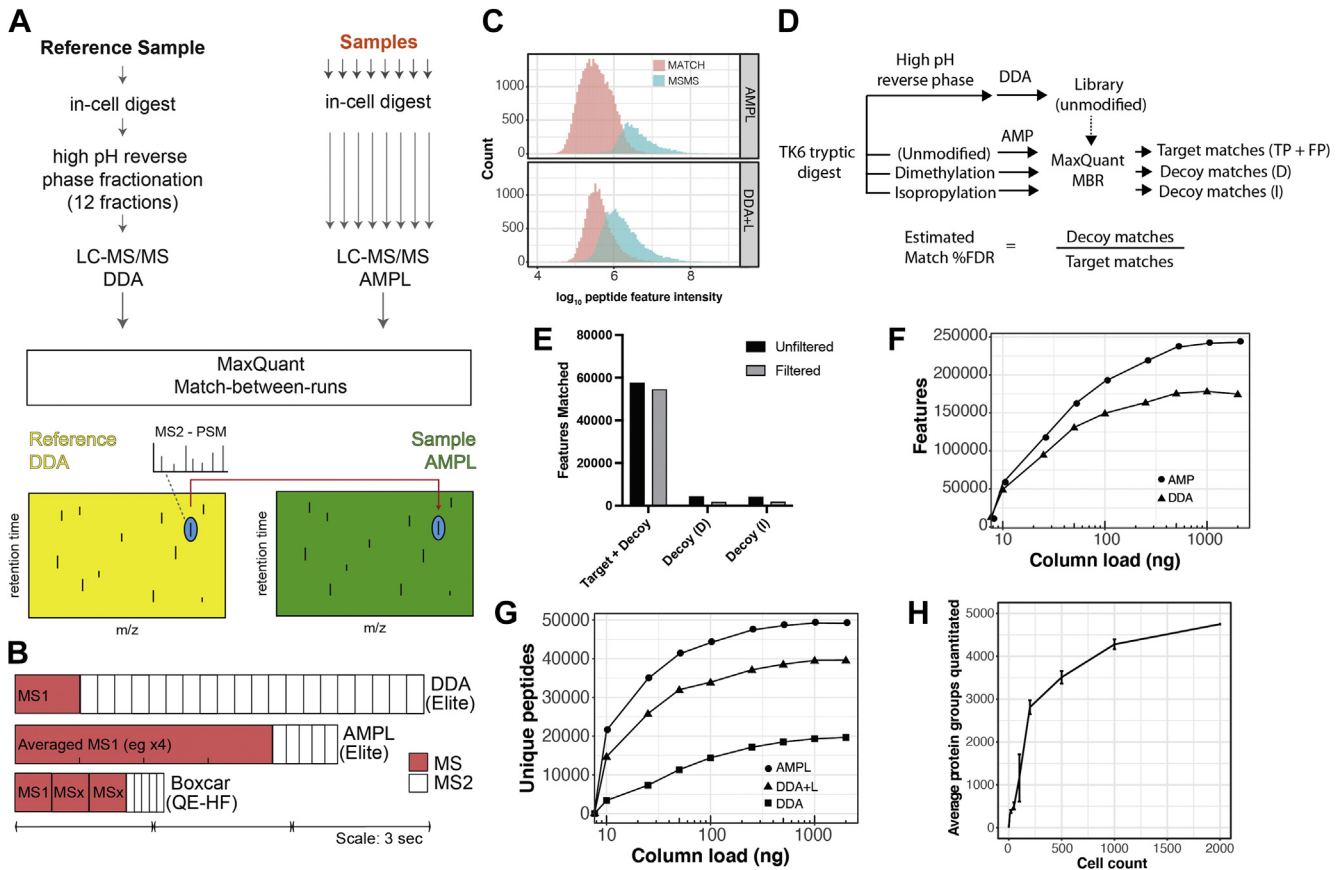


FIG. 2. Averaged MS1 precursor library matching (AMPL) increases peptide detection sensitivity. *A*, schematic outlining the AMPL experimental design. *B*, both the AMPL and BoxCar acquisition methods prioritize MS time to enhance MS1 scan quality. Schematic comparing duty cycles for data-dependent acquisition (DDA), AMPL, and BoxCar acquisition methods on the indicated MS instruments (Orbitrap Elite, Orbitrap HF). The median peak width using our chromatographic setup with the Orbitrap Elite is ~38 s. *C*, a comparison between AMPL and DDA + L, showing intensity distributions of peptide features identified by MS/MS (*blue*) and matching to identified library features (*red*). *D*, schematic outlining experimental workflow for assessing match-between-runs false discovery rate. *E*, features matched in target and decoy proteomes before and after additional filtering based on match retention time difference, match *m/z* difference, and match *m/z* error. *F* and *G*, features (*F*) and unique peptides (*G*) detected in AMP(L) versus DDA. DDA + L is DDA with matching to a library. *H*, proteome coverage versus cell number. The cell titration was performed in duplicate.

quenching with ammonium bicarbonate and desalting peptides over C18. About 200 ng of unmodified, dimethylated, and isopropylated peptides were analyzed by AMPL and DDA, and unmodified fractionated peptide samples were analyzed by DDA, as previously described. LC-MS data were searched using MaxQuant, as previously described. Note that dimethylation and isopropylation modifications were not specified in the search parameters.

Cell Cycle Proteomic Data Analysis

All subsequent data analyses on the protein intensity table, including the analysis of pseudoperiodicity, were performed using R (version 3.5.0) within the RStudio integrated development environment. The R scripts are available as [supplemental Data S1](#). The list of validated anaphase-promoting complex/cyclosome (APC/C) substrates was obtained from the APC/C degnon repository (<http://slim.icr.ac.uk/apc/>). Proteins that contain D box, KEN, and ABBA short linear (sequence) motifs (SLiMs) in the human proteome were found using SLiMsearch with default settings (disorder score cutoff: 0.30; flank length: 5). In order to remove slight variations in total protein

amount in each sample, protein intensities were divided by total intensities per sample and multiplied by 10^6 to obtain intensities in parts per million. There are four biological replicates analyzed in technical duplicate. As described previously, sample analysis was completely randomized in the second technical repeat. Each technical repeat (*i.e.*, set of four biological replicates) is considered as one “pseudotime-course” with samples in each biological replicate arranged in order from P1 to P16. Each of the two pseudotimecourse was then independently subjected to a Fisher’s test for periodicity, as implemented in the ptest R library (version 1.0–8). Fisher’s periodicity test *p* values were corrected for multiple hypothesis testing using the *q* value method as implemented in the qvalue R library (2.15.0). Those proteins that showed *q* values <0.10 in both sets of biological replicates and oscillation frequencies of either 0.0625 (1/16) or 0.125 (1/8) were classified as pseudoperiodic.

For clustering, protein parts per million values were averaged (mean) to produce a single pseudotimecourse for each protein. These average abundance profiles were scaled using the base R function scale and subjected to hierarchical clustering using the Ward minimum variance algorithm. The appropriate range for cluster

number was identified as 3 to 6 clusters using the “elbow method,” which involves plotting within-cluster sum of squares *versus* number of clusters. Bifurcating leaves of the subsequent dendrogram were swapped in order to produce a heatmap that follows a logical and sequential order of peak abundance, that is, cluster 1 with highest abundance in P0 to P8 and cluster 5 with peak abundance in P3 to P7, and others.

For principal component analysis (PCA) and CCS classification, scaled pseudotime courses were used. Cell cycle states were classified using the k-NN model as implemented in the class R library (version 7.3-15) using $k = 6$, with k being the number of nearest neighbors for classification. Three biological replicates were used as the training set, and the remaining replicate was used as a test set. R scripts used for this analysis can be found in [supplemental Data S2–S6](#).

RESULTS

The “In-Cell Digest”: Direct Protease Digestion of Fixed Cells

Based on previous work (1, 16), we hypothesized that formaldehyde-induced modifications were of low stoichiometry, and crosslink reversal may not be required for proteome analysis. Consistent with this idea, deep proteome analysis comparing human epithelial MCF10A cells fixed with 2% formaldehyde for 10 min, fixed and treated with heating to reverse formaldehyde crosslinks, or not fixed (Fig. 1A and supplemental Fig. S1A) showed no significant differences in protein and peptide coverage (Fig. 1, B and C). These proteomes were analyzed to a depth of ~53,600 peptides and ~7700 proteins. To identify peptides chemically modified by formaldehyde, we next used an error-tolerant MS search, which identifies peptide mass shifts in an unbiased fashion (supplemental Table S1) (17). The pattern and frequency of detected mass shifts are remarkably similar between control and fixed samples (supplemental Fig. S1B). From these observations, we concluded that under these controlled and mild fixation conditions, the stoichiometry of crosslinking and chemical modification by formaldehyde is sufficiently low such that the nondetection of modified and crosslinked peptides is not detrimental for characterization of proteomes to a depth of at least 7700 proteins.

We next hypothesized that fixed cells may make suitable substrates for direct protease digestion. Digestion of fixed cells would significantly simplify the sample processing workflow by eliminating several steps, including detergent-based lysis, homogenization, heat treatment, and detergent removal. We therefore treated fixed and permeabilized cells suspended in DPBS with either mock treatment (DPBS), or trypsin, and monitored cell morphology by brightfield microscopy. As shown in Figure 1D, prominent structural features visible in control cells, such as the plasma membrane, nuclei, and nucleoli, are degraded in a time-dependent manner by trypsin (supplemental Video S1). For LC–MS/MS analysis, fixed cells were also preincubated with benzonase to digest RNA and DNA oligonucleotides, which may interfere with downstream sample processing. The peptide-containing supernatant from the

digest was then subjected to C18 purification prior to analysis by LC–MS/MS. As the digestion occurs within the fixed cells, we have called this approach an “in-cell digest” (Fig. 1E).

As shown in Figure 1F, the proteome coverages are similar for fixed cells processed by the in-cell digest method (~4678 proteins, $n = 3$), fixed samples that were subjected to the PRIMMUS protocol (~4446 proteins, $n = 3$), and extracts from nonfixed cells processed by precipitation (see [Experimental Procedures](#) section, ~4561 proteins, $n = 3$). We conclude that the proteome coverage from the in-cell digest is similar, or higher, than the other protocols tested.

We did not observe a broad bias in quantitation, as label-free intensities measured in fixed cells prepared by the in-cell digest and by decrosslinking followed by an in-solution digest showed high correlation (Fig. 1G, $\rho = 0.96$). Similarly, a high correlation was observed between fixed cells prepared by the in-cell digest and nonfixed cells (Fig. 1H, $\rho = 0.97$). Few points lie off diagonal, indicating that proteins showing a major difference in intensity between methods are rare. We then tested if these off-diagonal proteins were enriched in any UniProt keywords or Gene Ontology annotations using DAVID. The only terms that were significantly enriched in proteins showing lower intensity with the in-cell digest were associated with RNA binding (FDR < 0.05; supplemental Fig. S1C). Notably, these RNA-binding proteins are present in cells at high abundance. In contrast, proteins showing higher intensity with the in-cell digest are enriched in membrane proteins (FDR < 0.05; supplemental Fig. S1D). Improved recovery of membrane proteins using the in-cell digest is consistent with previous results demonstrating that heat treatment can irreversibly precipitate membrane proteins.

We conclude that the measurements of protein abundance from the in-cell digest are quantitative, reproducible, and broadly comparable to conventional sample preparation methods. We note that each sample preparation method will have its own specific biases. In the case of the in-cell digest, the increased abundance of membrane proteins may more accurately reflect the abundance of these proteins in cells.

AMPL Improves Feature Detection

To increase the sensitivity and detection speed of the Orbitrap Elite MS instrument, we utilized MS1-based identification and quantitation using accurate mass and retention time matching, as proposed originally by the Smith laboratory (18). This approach has been recently demonstrated to be highly sensitive in an implementation called BoxCar (19). The BoxCar method increases the signal-to-noise (S/N) ratio of trap-based MS by collecting ions using segmented and spaced windows. Peptide identification relies on MS1 feature matching to a reference library generated from a fractionated reference sample using the MaxQuant function “Match-between-runs” (MBR). The library is analyzed separately using DDA, and peptides are identified by MS2 and database searches.

As the BoxCar method cannot be directly implemented on the Orbitrap Elite, we developed a different approach to increase the dynamic range of MS1 feature detection. MS1 spectral averaging is frequently performed in direct infusion MS but rarely employed in LC-MS bottom-up proteomics. We surmised that averaging several MS1 scans would improve S/N and would rapidly plateau as it is known that averaging improves S/N by a factor of \sqrt{n} , where n is the number of spectra averaged. Features would then be matched between the single shot analyses to a fractionated reference library (Fig. 2A). We call this method AMPL, or AMP if no library is used. Like BoxCar, AMP(L) prioritizes MS1 scans over MS2 scans as compared with DDA (Fig. 2B) and includes top-5 DDA MS/MS scans to ensure identification of features for accurate retention time alignment throughout the chromatographic separation.

We therefore tested AMPL by analyzing 1 μg on-column loads of MCF10A tryptic digests. A comparison of different MS1 scans ($n = 1, 3, 4,$ and 5) showed that the number of features and peptides identified saturates at $n = 4$ (supplemental Fig. S2, A and B). AMPL ($n = 4$) detects ~278,205 features, representing a 20% increase compared with a standard top 20 DDA acquisition using the same gradient (188,928 features). We reasoned that the additional peptides detected by AMPL originate from low-abundance features detected by virtue of the S/N increase because of averaging. Figure 2C compares the peptide intensity distributions between DDA-L and AMPL. The distributions are bimodal, with MS/MS-dependent identification biased toward higher intensity features (cyan). Consistent with the idea that AMPL improves S/N, AMPL detects a higher number of matched features (pink) in the low abundance regime. Similar to previous MS1-based matching approaches, AMPL shows higher data completeness (4411 proteins with intensities measured in all ten replicates) as compared with DDA-L (3493 proteins) and DDA (2865 proteins) (supplemental Fig. S2C).

MS1-based matching significantly increases the sensitivity, coverage, and data completeness of MS-based proteomics. However, the lack of MS2-based identification for these matched sequences could potentially increase the FDR. We estimated the matching FDR by using an empirical “target-decoy” approach, where decoy proteomes created by chemical modification (dimethylation and isopropylation) are matched against an unmodified library (Fig. 2D). Whereas matches to the target proteome will contain both true and false positives, matches to the decoy proteomes should contain exclusively false positives (with the rare exception of peptides containing an N-terminal acetyl group, a C-terminal arginine, which are not dimethylated/isopropylated). About ~32% of the features are assigned a peptide sequence when the target and unmodified proteome is matched against an unmodified library (supplemental Fig. S2D). By contrast, only ~2% of the features are matched in the decoy samples (supplemental Fig. S2D). Using this approach, the estimated

match FDR is 7.4%. To reduce the FDR to <5%, we applied additional thresholds for match time, match m/z , and match m/z error (2.5σ for match time, 3σ for match m/z and match m/z error, supplemental Fig. S2, E and F). Application of these thresholds reduced the estimated FDR to 3.1-3.4% (Fig. 2E) while retaining 96% of the matches in the target dataset.

The improvements in detecting low abundance features suggest that AMPL may be well suited to analysis of low sample loads. AMP (*i.e.*, no library) consistently detects more features than DDA (Fig. 2F), which leads to significant improvements in peptide coverage (Fig. 2G). For example, at 10 ng loading, 21,483 unique peptides are quantitated by AMPL *versus* 14,702 by DDA-L, representing a 46% increase in coverage. AMPL provides 150 to 535% improvement relative to conventional DDA with no library and 24 to 46% improvement relative to DDA-L for protein coverage at all tested column loads with greatest gains observed at low column load.

As shown in Figure 2G, AMPL detects a slightly higher number of peptides in 10 ng on-column load as DDA with 1 μg load, demonstrating a >100 \times increase in sensitivity. A 10 ng on-column load is equivalent to the protein content of ~67 cells based on the protein per cell measured in bulk assays. However, the effective number of cells required for proteome analysis is frequently much higher due to losses during sample preparation. We reasoned that these losses are significantly reduced using the streamlined in-cell digest.

We combined the in-cell digest with AMPL to analyze FACS collected TK6 cells, a human lymphoblastoid cell line (LCL) with a stable near-diploid karyotype. Notably, TK6 cells are smaller than typical adherent human cell lines, such as HeLa and MCF10A. Being cultured in suspension, TK6 cells are amenable toward cell separation techniques, including FACS and centrifugal elutriation, without requiring cell dissociation, which can induce physiological perturbations.

Figure 2H shows the result of a cell titration analysis of S-phase cells performed in duplicate, whereby two aliquots at each indicated cell number (2000 cells to 0 cells) were collected by FACS from the same starting cell population. Approximately, 4500 proteins were quantitated with 2000 cells, with 4480 proteins reproducibly quantitated in two technical repeats. At the lower end of the cell titration, 2933 proteins on average were quantitated from 200 cells. We note that below this number of cells, we observe a higher variability in proteome coverage, which will need to be addressed by further optimization. Indeed, while approximately 30 proteins were detected in single cells, with 17 reproducibly detected, nearly all these proteins were also detected in the background samples (“0 cells”).

We conclude that combining in-cell digest and AMPL enables characterization of proteomes of 2000 cells to a protein depth comparable to conventional single shot DDA analysis of

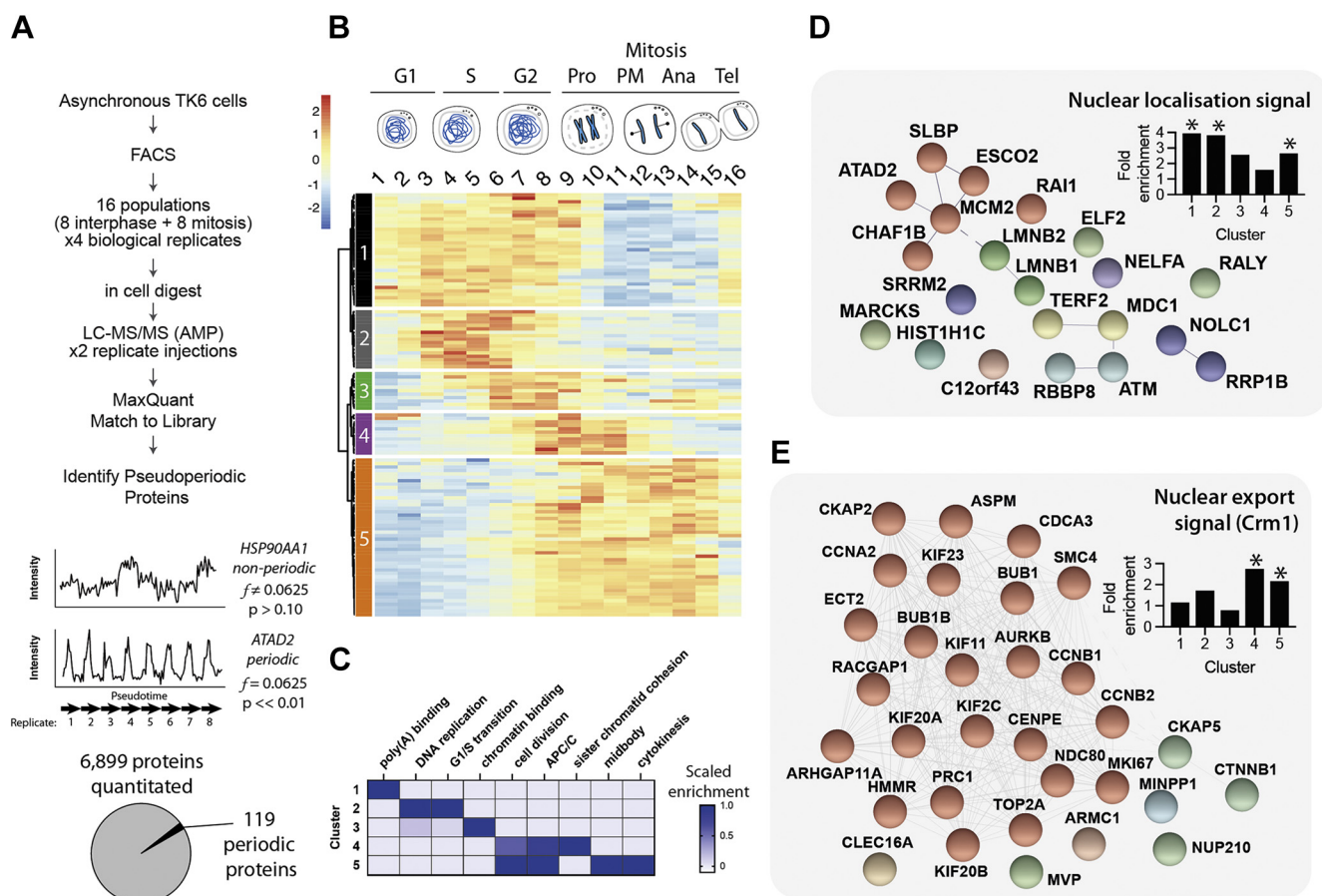


FIG. 3. High-resolution proteomic analysis of an unperturbed cell cycle. *A*, schematic describing the experimental design and workflow. Details for protein abundance normalization and pseudoperiodicity analysis can be found in the [Experimental Procedures](#) section. *B*, heatmap of the 119 identified pseudoperiodic proteins organized by cluster. Schematic above heatmap shows indicative cell cycle stages isolated by FACS (full gating strategy is shown in [supplemental Fig. S3](#)). *C*, enriched UniProt keywords by cluster. *D*, proteins in clusters 1 and 2 containing a putative nuclear localization signal (NLS). *E*, proteins in clusters 4 and 5 containing a putative nuclear export signal (NES). * indicate $p < 0.01$ (Fisher's exact test). FACS, fluorescence-activated cell sorting.

1 μ g on-column loads. The advanced PRIMMUS method presented here significantly reduces the number of cells required, that is, $\sim 10^3$ versus $\sim 10^5$ with low estimated match FDR ($< 3.5\%$).

High Temporal Resolution Analysis of an Unperturbed Cell Cycle Using PRIMMUS

The process of normal cell division requires linear progression through several cellular states (*i.e.*, S and M phases) in which DNA replication and mitosis must occur in sequential order. These states can be further resolved. DNA replication, for example, occurs in a temporally and spatially patterned manner, with euchromatic genomic regions replicating first before heterochromatin-dense regions. Similarly, M phase can be resolved into prophase, prometaphase, metaphase, anaphase I, anaphase II, and telophase based on cytological features. Some of these phases, including telophase, are exceptionally rare in asynchronous cells and are not amenable for collection by FACS in numbers required for typical

proteomic analysis. We therefore developed an advanced PRIMMUS workflow incorporating the in-cell digest to target these rare cell states and carry out a high temporal resolution analysis of proteome variation across 16 cell cycle sub-populations, including eight interphase and eight mitotic states ([Fig. 3A](#)). This fractionation-based approach to separating cell cycle phases relies on continuous cell trajectories, such as cell cycle progression in asynchronous populations that are unperturbed by drug-based synchronization.

TK6 cells were immunostained for DNA content, cyclin B, cyclin A, and histone H3 phosphorylation (Ser28), which are all markers of cell cycle progression. Cells were then separated into 16 cell cycle populations (P1–P16) (see [supplemental Fig. S3](#) for the full gating strategy). Biochemical differences are used as a surrogate for time and cell cycle progression. Based on the past literature ([20, 21](#)) and our previous data ([1](#)), we have correlated these biochemical changes with specific CCSs (as illustrated in [Fig. 3B, top](#)). For example, cyclin A and cyclin B levels are used to discriminate mitotic subphases, as

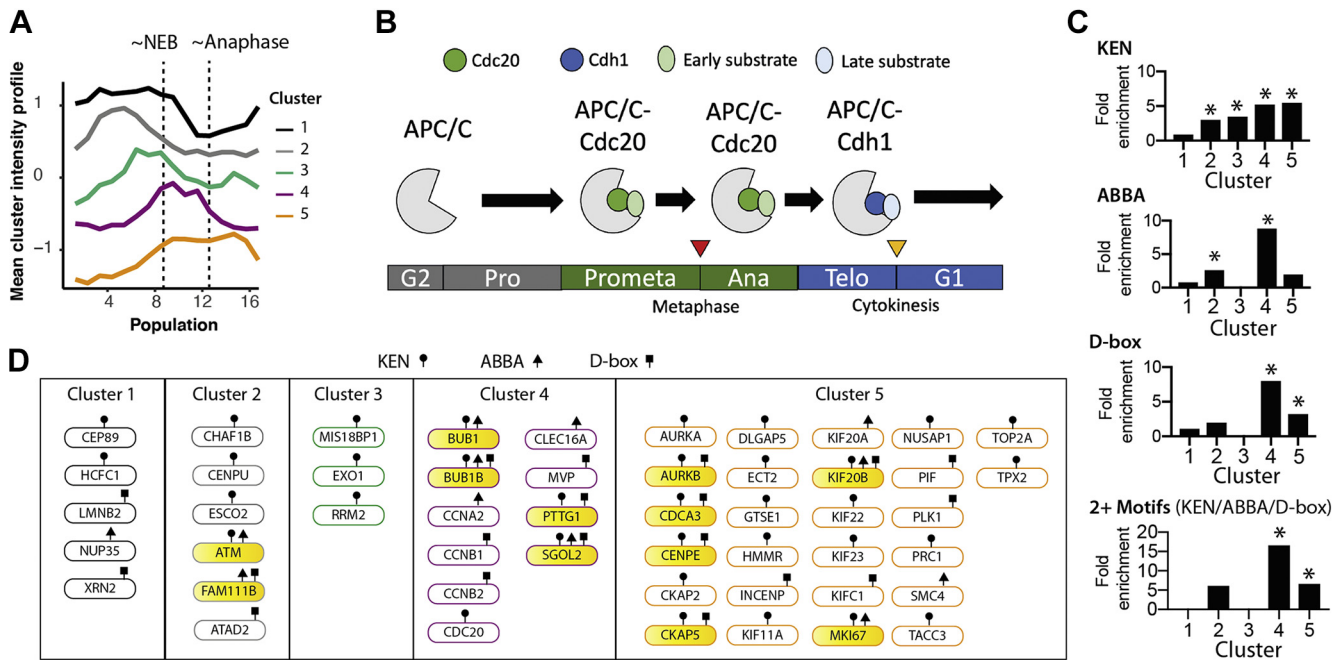


FIG. 4. **Characterization of potential APC/C substrates.** A, mean intensity profile for five clusters is shown in Figure 3B. B, schematic illustrating regulation of APC/C substrate choice switch during mitosis by coactivators Cdc20 and Cdh1. C, enrichment analysis of SLiMs that control interaction with the APC/C. D, proteins with at least one APC/C SLiM grouped by cluster. The yellow fill indicates proteins that contain two or more SLiMs. APC/C, anaphase-promoting complex/cyclosome; SLiM, short linear (sequence) motif.

they are degraded during prometaphase and the metaphase-to-anaphase transition, respectively. Proteome characterization of these cells, previously challenging because of lack of sensitivity, is now possible with the in-cell digest.

The rarest target population are cells in late anaphase of mitosis, which are present in 0.01% of an asynchronous TK6 culture. Four separate cultures of TK6 cells were independently FACS separated into 16 populations. For each population, 5000 cells were collected and processed using the in-cell digest. Collection of 5000 cells provided sufficient material for duplicate injections for LC-MS/MS analysis by AMPL with DDA libraries generated from interphase, mitotic, and asynchronous cells. The data were then processed by MaxQuant with MBR (supplemental Table S2) and filtered by match parameters as discussed previously to generate a dataset with 7553 quantitated proteins (supplemental Table S3).

Next, to identify cell cycle-regulated proteins, we treated each set of 16 populations as an ordered series of biochemical states. These states were projected onto a temporal axis (*i.e.*, cell cycle progression). A single replicate series of ordered cell states constitutes a “pseudotimecourse” (Fig. 3A, bottom). We then applied the Fisher’s periodicity test to identify “pseudoperiodic proteins” (PsPs), that is, protein abundance patterns that showed periodic behavior across the four pseudoperiodic timecourses. In order to increase robustness, the periodicity test was separately performed on each technical repeat, and only those proteins showing periodicity in

both were designated as PsPs. Figure 3A (bottom) shows the abundance profiles for heat shock protein HSP90AA1 and ATPase AAA domain-containing protein ATAD2 as an example non-PsP and PsP, respectively. ATAD2 shows highly reproducible abundance variation in all eight pseudotimecourses, with peak abundance in S-phase populations (P5–P6), consistent with previous reports (22). In total, 119 PsPs were identified using these criteria (Fig. 3A, bottom, supplemental Table S4).

Hierarchical clustering of the 119 PsPs identified five major classes of protein abundance patterns (Fig. 3B). Each cluster shows peak abundance at different times during cell cycle progression. The Gene Ontology terms enriched for each cluster reflects key processes and/or compartments associated with the respective phase of the cell cycle (Fig. 3C). We also assessed enrichment in SLiMs. SLiMs mediate protein–protein interactions that lead to changes in post-translational modification, stability, and/or subcellular localization of a protein. Using the eukaryotic linear motif database (23), we identified SLiMs that are enriched in each cluster ($p < 0.01$, Fisher’s exact test, supplemental Table S5).

Cluster 1 proteins show high abundance in interphase, which decreases in early mitosis (P8–P10) and recovers slightly in late mitotic populations (P15–P16). This cluster is highly enriched in proteins with a monopartite nuclear import signal sequence (Fig. 3D), and in contrast to other clusters, do not show any enrichment for the Crm1-mediated nuclear export signal (NES) sequence (Fig. 3E). Most proteins in this

cluster are either RNA or DNA binding (26/33). For example, several mRNA splicing factors are in this group, including serine/arginine-rich proteins (SRRM2, SRSF2, SRSF3, SRSF5, SRSF6, and SRSF10/TRAB). These proteins reproducibly decrease in abundance in mitosis, but with a small fold change (less than twofold) than key cell cycle regulators, for example, cyclin B1 (greater than fourfold). The stability of the SR proteins is regulated by nucleocytoplasmic shuttling. For example, SRSF1 is stable in the nucleus but has a short half-life in the cytoplasm (24). Proteasome-dependent degradation of SR proteins is dependent on the RS domain, which is shared among SR proteins (25). Cluster 1 is also enriched in poly(A)-binding proteins in the nucleus that are involved in pre-mRNA and ribosomal RNA processing, for example, XRN2, NOLC1. The remaining proteins with no known or anticipated oligonucleotide-binding properties are enriched in cytoskeleton-binding factors, for example, the actin-binding protein MARCKS, CCDC6, CEP89, and DBNL.

Cluster 2 proteins peak in late G1/S. Nearly all proteins in this cluster are directly involved in DNA replication, establishment of nascent chromatin, or the G1/S transition (Fig. 3C). In this cluster are three members of the MCM helicase (MCM2, MCM5, and MCM6), the replication-dependent histone chaperone (CHAF1B), and the histone mRNA stem-loop binding factor SLBP, which is essential for the synthesis of histones for incorporation into newly synthesized DNA in S phase. This cluster also includes the DNA damage checkpoint kinase ATM, which is important in resolving endogenous replication stress (26).

Cluster 3 shows peak abundance in late S, G2 (P6–P8), and decreased abundance in early-mid mitosis (P9–P11). Three proteins show greater than fivefold decrease in abundance by mid-mitosis with low or undetectable levels in late mitosis: GMNN, RRM2, and PAF/KIAA0101. All three are targeted for degradation in late mitosis and G1 by the APC/C-Cdh1. The remaining proteins in the cluster show an increase in S/G2 phase and a decrease in prophase/prometaphase (P9–P12), followed by a slight recovery in abundance in late mitosis. These include sororin/CDCA5, which functions in sister chromatid cohesion establishment, and MIS18BP1, which facilitates loading of the centromere-specific histone in late mitosis and G1. This cluster is enriched in chromatin-binding factors, including TRIM28/KAP1, EXO1, sororin, PAF, and MIS18BP1.

Clusters 4 and 5 show peak abundance during mitosis and contain the largest proportion of proteins with either known direct roles in mitotic progression or targeted for degradation in mitosis (9/12 for cluster 4 and 38/46 for cluster 5). The feature that distinguishes clusters 4 and 5 is the mitotic abundance pattern. Cluster 4 proteins show decreased abundance in earlier mitotic populations, particularly in P11 to P12, coincident with the onset of cyclin A2 and cyclin B1 degradation. The three mitotic cyclins detected (A2, B1, and B2), the spindle assembly checkpoint

kinases BUB1 and BUB1B (BubR1), the kinesin-8 family member KIF18B, securin (PTTG1), and shugoshin (SGO2) are in this cluster. Functionally, this cluster is characterized by proteins that 1) protect sister chromatid cohesion (securin and shugoshin) and, 2) form the spindle assembly checkpoint (Bub kinases), which prevents anaphase while proper microtubule attachment and biorientation of chromosomes takes place.

By contrast, cluster 5 proteins show a significant increase in abundance at the end of interphase (P7–P8) with peak abundance throughout mitosis (P9–P15) and a significant decrease only in the last population (P16), that is, cells undergoing mitotic exit. Example proteins include the catalytic E2 subunits of the APC/C (UBE2C and UBE2S), the chromosome passenger complex (AURKB, INCENP, BIRC5–survivin, CDCA8–borealin), polo kinase (PLK1), and the spindle-associated protein FAM83D. Both aurora kinases (aurora A and aurora B) are known to relocalize to the central spindle after anaphase onset. Aurora B activity is crucial for cytokinesis, the final step in cell division.

Clusters 4 and 5 are strongly enriched in the Crm1-mediated NES (Fig. 3E). About 8/12 proteins in cluster 4 match the NES consensus. Notably, cluster 4 includes cyclins B1 and B2, and constitutive export of cyclin B–cyclin-dependent kinase from the nucleus is important in preventing premature mitotic entry. Exclusion from the nucleus of other proteins within these two clusters (Fig. 3E) may also be important in preventing premature activation of processes that are normally restricted to mitosis.

We identified PsPs that have no reported function in cell cycle control. These novel cell cycle-regulated proteins may, like many of the other proteins identified in this manner, have significant roles in cell cycle progression. These candidates include EXO1, the DNA helicase PIF1, the guanine-exchange factor NET1, and the serine protease FAM111B.

Analysis of Mitotic Protein Abundance Dynamics in Unperturbed Cells

A major difference between the clusters is the timing of protein abundance decrease (Fig. 4A). A critical regulator of protein abundance during the cell cycle is the APC/C. The APC/C is an E3 ubiquitin ligase and is active during the mitotic and G0/G1 phases of the cell cycle (27, 28). Its substrates include key regulators of the cell cycle, including cyclin A2 and cyclin B1. Ubiquitination of APC/C substrates is tightly temporally controlled, with APC/C substrate specificity changing during the cell cycle (Fig. 4B). This is mediated through changes in the APC/C coactivators and substrate recognition factors, Cdc20 and Cdh1. While APC/C-Cdc20 is active in early mitosis, the substrate receptor changes to Cdh1 in late mitosis, thereby conferring a temporal order to substrate degradation. Cdc20 is itself a substrate of the APC/C-Cdh1, allowing for switch-like handover in substrate receptor control.

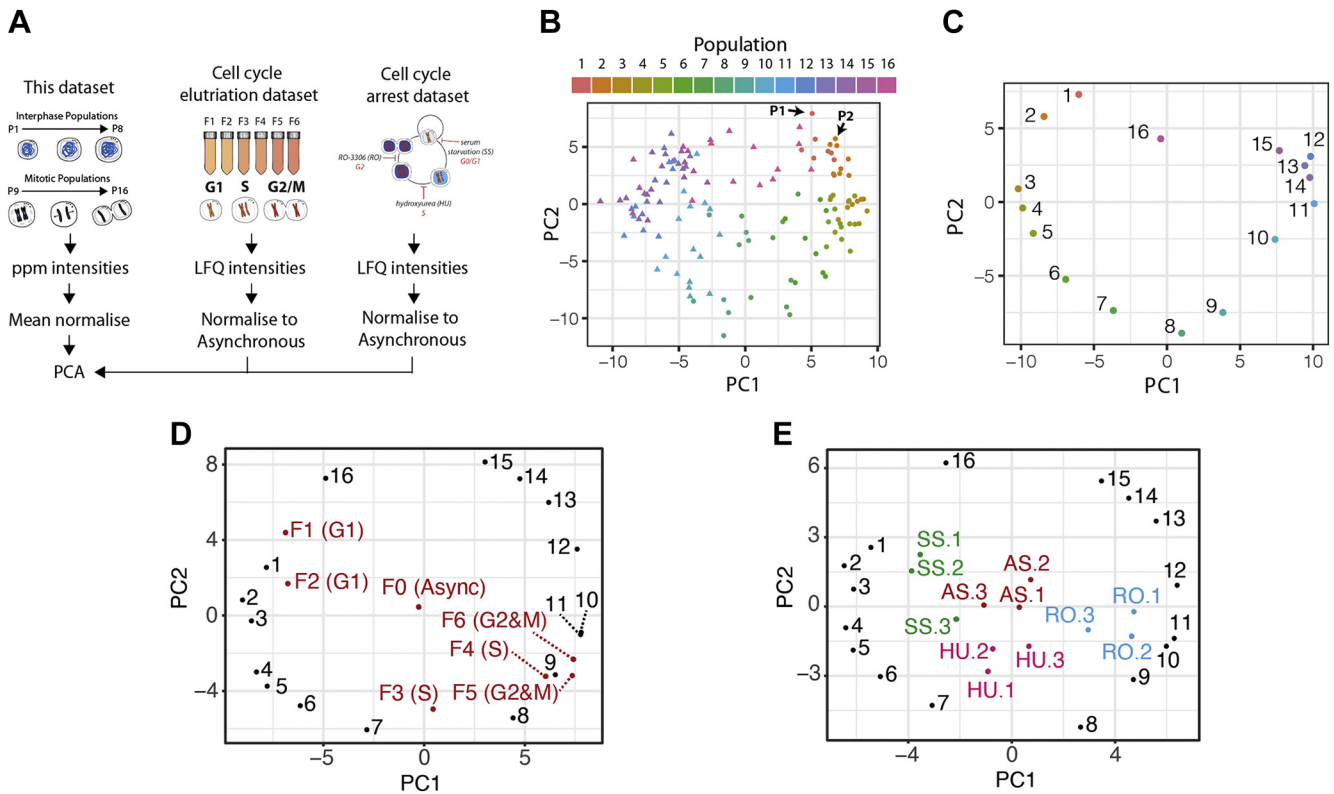


FIG. 5. **The 119 PsPs form a signature that classifies cell cycle states.** A, schematic illustrating the approach to compare the signature across datasets. B and C, PCA of the 16 cell cycle populations in this study using the 119 PsPs as features using either individual replicates (B) or mean abundances (C). D and E, PCA as in (C) with samples from elutriated (D) or from cell cycle arrest (E) label-free datasets using NB4 cells. AS, asynchronous; HU, hydroxyurea; PCA, principal component analysis; RO, RO-3306; SS, serum starvation.

About 25 PsPs (out of 119) are experimentally validated APC/C substrates (29), and of these, 24 are found in clusters 3, 4, and 5. Substrate recognition by APC/C-Cdc20 and APC/C-Cdh1 is mediated by the interaction between WD40 domains on the APC/C-(Cdc20/Cdh1) and SLiMs found on substrates. The KEN and D-box (RxxL) degrons are well-documented SLiMs that bind both APC/C-Cdc20 and APC/C-Cdh1, with APC/C-Cdh1 having a preference for the KEN degron. A third SLiM called the ABBA motif was shown to be important in substrate recognition by APC/C-Cdc20 (30).

Figure 4C shows the enrichment profile of these SLiMs across the six clusters. The KEN motif is comparably enriched in four of the five clusters (Fig. 4C, top), with highest enrichments for the mitotic phase-peaking clusters (clusters 4 and 5). The frequencies range from 25% of the proteins in a cluster having the KEN motif (cluster 2) to 43% (cluster 5), representing a threefold to fivefold enrichment over the background frequency (8%). All four clusters show low to nondetectable abundance in P16, P1, and P2, that is, mitotic exit and G0/early G1 when APC/C-Cdh1 is active. In total, 35 cell cycle-regulated proteins contain a KEN SLiM, approximately 50% (18 proteins) that have been experimentally characterized as APC/C substrates. The remaining uncharacterized 17 proteins are excellent candidates to be APC/C-Cdh1

substrates. Consistent with this prediction, cluster 1, which is the only cluster showing no enrichment for the KEN motif, contains proteins that have on average, higher abundance in G0/early G1.

Six of 12 proteins that peak in mid-mitosis (cluster 4) contain the RxxL D-box sequence. The 50% frequency is approximately eightfold higher than the background frequency (6%). By contrast, the fold enrichment is considerably lower in the other clusters (Fig. 4C). Similarly, five of 12 proteins contain the ABBA motif (42%; Fig. 4C), representing an approximately ninefold enrichment over the background frequency (5%). D-box and ABBA motif-containing proteins in this cluster are mostly mutually exclusive (Fig. 4D). Of the D-box and ABBA motif-containing proteins, two have not been previously experimentally characterized as APC/C substrates: MVP and CLEC16A.

Cluster 4 is highly enriched in proteins containing more than one SLiM (KEN/D-box/ABBA; Fig. 4C, bottom), and two proteins in this cluster contain all three SLiMs: BubR1 (BUB1B) and shugoshin-2 (SGOL2). KIF20B is the only other PP that has all three SLiMs and is in cluster 5. BubR1 has been demonstrated to interact with APC/C through these three SLiMs and acts as a pseudosubstrate to inhibit APC/C activities in spatiotemporally controlled manner (31). It would be

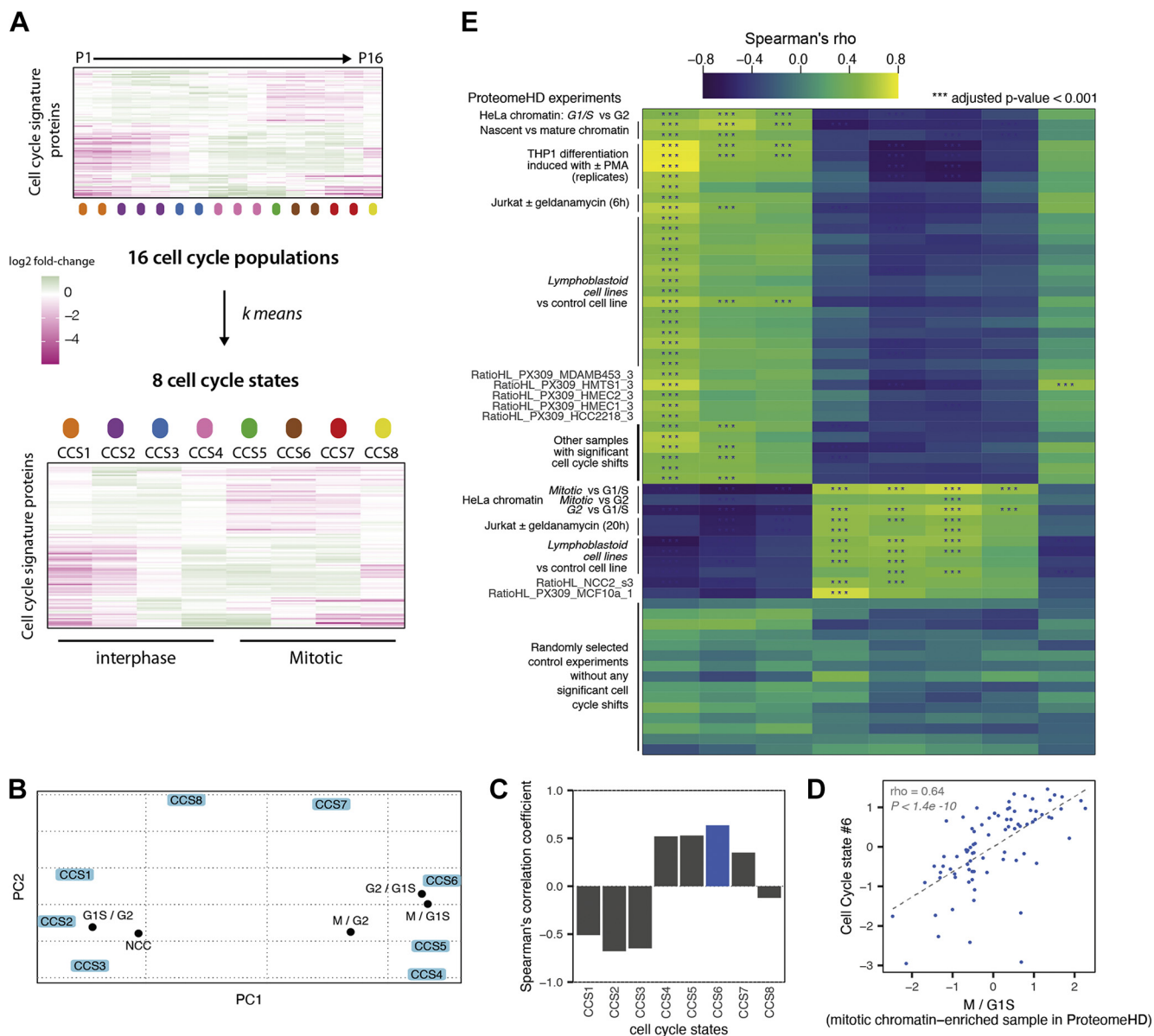


FIG. 6. Unbiased assignment of CCSs across hundreds of proteomes in ProteomeHD. *A*, schematic of how the 16 cell cycle populations were aggregated into eight CCSs. *B*, assignment of chromatin proteomes from nascent chromatin capture (NCC) and chromatin enrichment proteomics (ChEP) SILAC experiments. NCC samples were enriched in S phase. G1S, G2, and M samples were treated with thymidine, RO-3306, and nocodazole, respectively. *C*, Spearman rank correlation coefficient for the eight CCSs for M/G1S. This sample has the highest correlation with CCS6 (blue fill). *D*, correlation scatter plot between CCS6 and M/G1S. *E*, heatmap showing Spearman correlation coefficients for 47 experiments (out of 294) that show an enriched CCS and 15 randomly selected experiments that have no CCS enrichment. The columns shown are CCS1 to CCS8. CCS, cell cycle state; SILAC, stable isotope labeling by amino acids in cell culture.

interesting to test the role of these SLiMs in the other two proteins (SGOL2 and KIF20B). For example, SGOL2 has functions in protecting sister chromatid cohesion and in the spindle assembly checkpoint (32).

Proteomic Assignment of CCSs

MS-based single-cell proteome analysis is an emerging area. Recent advances in miniaturized sample preparation (5, 9–11) suggest that routine proteome analysis of single

somatic mammalian cells will be possible in the near future. In comparison, single-cell transcriptomics as a mature field with commercial kits is now available. In single-cell RNA-Seq analysis (33), the deconvolution of CCS has been critical (34, 35). This is because cell cycle variation contributes significantly to the variation observed in a cell population. For example, to identify cell fate trajectories during differentiation, researchers relied on reference cell cycle-regulated genes in order to identify the effect of cell cycle variation in the gene

expression differences observed (36). A validated reference set of cell cycle–regulated proteins will be important for the biological interpretation of single cell proteomic datasets.

We tested whether the abundances of the PsPs determined in this study were sufficient to assign specific CCSs to cellular proteomes (Fig. 5A). The abundance patterns for the 119 proteins for each sample (16 time points \times eight replicates = 128 samples) were subjected to PCA. The two major PCs, PC1 and PC2, explain 53% and 20.5% of the variance, respectively, as shown in Figure 5B. Interphase (*circles*) and mitotic (*triangle*) phases are separated predominantly along PC1. To a lesser extent, subphases within each (*e.g.*, see *arrows* indicating P1 and P2) are separated along both PCs. Moving counterclockwise, starting from the top right for P1, the samples clearly follow a trajectory that reflects the position of each sample in the cell cycle, starting from early G1 (P1 and P2) to mitosis (*left side, triangles*). Telophase/cytokinesis populations (P16, *pink triangles*) are situated between the other mitotic populations and P1. To ease visualization, the PCA was repeated using mean values per population (Fig. 5C). Using unbiased and unsupervised methods, the PCA has arranged the populations into a cell cycle “wheel,” suggesting a largely continuous process with the major separation along PC1 correlated with interphase (P1–P8) *versus* mitosis (P9–P16). It is less clear what is the major correlate for PC2. We note however that there is a correlation with APC/C activity, with active APC/C in populations with positive values along PC2 (early G1 and end of mitosis) and inactive APC/C in populations with negative values (S and G2).

Detection of relevant features is essential as PCA analysis of the entire proteome dataset does not result in cell cycle separation. Repeating the PCA analysis with cyclin A2 and cyclin B1 removed essentially produces identical results, which indicates that the relationships produced by using ~119 cell cycle marker proteins are robust toward the absence of individual proteins, including key proteins that drive cell cycle progression. This robustness will be important in assigning CCSs in diverse datasets, as described later.

We then asked whether the PCA classification could be used to assign CCSs to cellular proteomes obtained in published cell cycle fractionation and arrest experiments. Human promyelocytic leukemia cells (NB4) were fractionated by centrifugal elutriation into different cell cycle populations (Fig. 5A, *middle*) (37). There are seven fractions (F0–F6), which correspond to asynchronous (F0), and samples enriched in G1 (F1–F2), S (F3–F4), and G2&M (F5 and F6). In a separate experiment, NB4 cells were arrested in G0 phase, S phase, and G2 phase, respectively, using serum starvation, hydroxyurea, and the CDK1 inhibitor RO-3306 (RO) (Fig. 5A, *right*) (2). Label-free quantitation intensities were normalized to asynchronous cells, and these ratios were combined with mean-normalized data from this dataset prior to PCA.

Figure 5, D and E shows the combined PCA plots for the elutriation and arrest datasets, respectively. The NB4 cell populations are broadly separated according to the appropriate cell cycle phase. For example, as shown in Figure 5D, F1 and F2 are positioned nearby P1 (early G1). F3 is in between P7 and P8 (late S/G2), and F4 is near P9 (late G2/early mitosis). F5 is closest to P9, whereas F6 is in between P9 and P10 (late G2/early mitosis). In Figure 5E, the serum starvation samples are nearest the early G1 populations, P1 to P4. The hydroxyurea samples are in between P7 and P8, which are late S/G2 populations. The RO samples are positioned near P9 to P11, which are late G2/early mitotic populations. We conclude from these data that this signature can be used to classify cell cycle–enriched label-free proteomes.

We next tested if the cell cycle signature can be broadly applicable to assign CCS to a proteome. To do this, we made use of a large set of stable isotope labeling by amino acids in cell culture (SILAC) datasets curated in proteomeHD (38). Incomplete synchrony and/or cell cycle enrichment will generally lead to much poorer purities compared with FACS. This lowers the resolution of classification for bulk population samples, which likely contain mixtures of different phases unless purified by FACS. This will not be the case for single-cell proteomes, which will be by definition in a single-cell state.

To facilitate assignment of CCSs to partially or completely asynchronous bulk populations, we first used k-means clustering to reduce the number of classes from 16 populations to eight CCSs (Fig. 6A and supplemental Table S6). PCA using these eight CCSs also shows the cell cycle “wheel” (Fig. 6B). We then mapped chromatin proteomes (nascent chromatin capture [NCC] and chromatin enrichment proteomics) from synchronized cells, arrested with thymidine (G1/S), 3 h thymidine release (NCC), RO (G2), or nocodazole (M) (Fig. 6B). Although these samples were from a different cell type than our cell cycle signature data (HeLa *versus* TK6) and had been processed differently (chromatin-enriched *versus* in-cell digest) as well as quantitated differently (SILAC *versus* label free), these samples group according to the appropriate cell cycle phase. For example, the G2 and M-phase samples are grouped between CCS6 and CCS5, which are early-to-mid mitotic states. By contrast, G1/S and NCC samples are grouped with CCS2 and CCS3, which are G1/S states.

One challenge for the systematic classification of a heterogeneous set of proteomics data are missing values, because not all our 119 signature proteins were detected in all experiments in ProteomeHD. We therefore employed Spearman rank correlation to correlate the abundance of the signature proteins in these chromatin proteomes with the eight CCSs. For example, the M/G1S proteome shows the highest correlation with CCS6 (Fig. 6, C and D), which is a mitotic state.

We subsequently applied this correlation approach systematically to all 294 experiments in ProteomeHD. We found that ~15% of the experiments in ProteomeHD (47 of 294) showed a high and significant correlation with one or more CCS (supplemental Table S7). Many of these experiments involve a cell cycle perturbation, including the NCC and chromatin enrichment proteomics experiments described previously (Fig. 6, B–D). These experiments also include other types of perturbations, including differentiation, where cell cycle arrest is an expected direct consequence. For example, proteomes from THP-1 monocytic cells treated with phorbol myristate acetate ester are highly correlated with G1 CCSs. Phorbol myristate acetate treatment induces terminal differentiation of these cells and leads to cessation of cell proliferation. In total, ~50% of the proteomeHD experiments highly correlated with a CCS can be linked directly to cell cycle arrest.

From these data, we conclude that the signature robustly and accurately assigns CCS across far ranging experimental contexts, cell types, and quantitation strategies.

The remaining experiments with high correlation have less obvious links to cell cycle. For example, Jurkat T cells are treated with the HSP90 inhibitor geldanamycin for either 6 h or 20 h (Fig. 6E). Proteomes from 6 h treatment are highly correlated with CCS1 (early G1). By contrast, proteomes from 20 h treatment are highly correlated with the G2/mitotic states, CCS4 and CCS6. Geldanamycin has been reported to arrest cells in G1 or G2 phases of the cell cycle. Interestingly, flow cytometry analysis of cells treated with geldanamycin for 20 h shows an accumulation of 4N DNA content cells, corresponding to G2&M phase cells (39).

We also detect significant CCS signatures in experiments that have no apparent link to cell cycle arrest, direct or indirect. In a study comparing untransformed breast epithelial cells with breast cancer cell lines, three untransformed breast epithelial lines, MCF10A, HMT-3522, and HMEC1, showed significant correlation with one or more CCS. Cell lines were compared using a super-SILAC approach against MCF7, which is a hormone receptor-positive breast cancer line. Both HMT-3522 and HMEC1 show strong correlation with early G1 states (CCS1). By contrast, MCF10A was correlated with S phase (CCS4). Interestingly, MDA-MB-453 cultures also showed correlation with CCS1. These data suggest that the cell cycle distributions of these cell cultures are shifted compared with MCF7. In a separate study, 16 of 62 LCLs analyzed by proteomics to identify quantitative trait loci were significantly CCS correlated (Fig. 6E). Interestingly, they were correlated in different states: 12 correlated with CCS1 and/or CCS2 (G1 phase) and the remaining four correlated with CCS5 (G2/early mitosis). These data suggest that there is significant heterogeneity in cell cycle distribution, impacting at least 25% of the LCLs compared. How much of the heterogeneity in CCS correlation observed has a genetic basis

or is due to technical variation in cell culture handling will be important to assess.

DISCUSSION

A major challenge with the comprehensive analysis of proteomes from low cell number samples is sample preparation. An on-column load of 200 ng peptide, the equivalent to the protein content of approximately 2000 TK6 cells, is sufficient material to obtain proteome coverage of >4000 proteins with current instrumentation. Removal of detergents used to produce soluble cell extracts by use of membrane filters (6), organic precipitation (with or without the aid of magnetic beads) (7, 40), or SDS-PAGE gel extraction are protocols involving several steps and repeated exposure to new plastic surfaces that introduce opportunities for nonspecific peptide and protein adsorption. Here, we have presented a minimalistic approach for preparing cells for proteomics called the “in-cell digest.” Cells are fixed with formaldehyde and methanol to effectively trap them in biochemical states, then directly digested with trypsin, and desalted prior to LC-MS/MS analysis.

We show that the in-cell digest enables reproducible and quantitative analysis of proteomes from 2000 TK6 and MCF10A cells using AMPL analysis. The AMPL approach overcomes the low duty cycle of the Orbitrap Elite to enable proteome analysis with a sensitivity comparable with current instruments. Newer instrumentation with higher duty cycles, including the TIMS-TOF Pro and Exploris 480, is expected to enable conventional DDA and data-independent acquisition analyses of proteomes at a similar depth with 2000 TK6 cells, or alternatively, improve proteome depth further using MS1-based matching methods.

The in-cell digest is compatible with other approaches of low cell number sample preparation for MS-based proteomics. In-cell digested samples can be efficiently labeled by isobaric tags, for example, tandem mass tag and isobaric tag for relative and absolute quantitation, and therefore compatible with use of carrier channels to boost the signal of rare or single cell channels (e.g., iBASIL (41)). The protocol requires no specialized humidified sample handling chambers or direct loading onto premade analytical nanoLC columns, such as those described in the nanoPOTS workflow (11). While the proteome coverages obtained by nanoPOTS is higher than reported here, it is possible that a new workflow combining aspects of the in-cell digest and nanoPOTS could improve both generalizability and performance compared with either method.

Each sample preparation method will have its unique advantages and potential biases, which we evaluated by quantitatively comparing the in-cell digest with a more conventional in-solution digest. This analysis revealed an overrepresentation of membrane proteins amongst those proteins

with higher abundance measured in the in-cell digest samples. These proteins include mitochondrial membrane proteins (e.g., TOMM7) and proteins that are known to be localized to the cell surface (ADAM15). Membrane proteins have been shown to irreversibly aggregate in soluble extracts when heat treated and precipitated. Delipidation by methanol, which is used to increase cell permeability, could also play an important role in increasing digestion efficiency of membrane proteins by trypsin. We suggest that the higher abundances measured for membrane proteins is unlikely to be an artifact of the in-cell digest; in contrast, the measurements are likely to more accurately reflect the abundances of these proteins in cells.

Feature matching FDR is controlled in our approach by implementing stringent cutoffs for retention time difference, m/z difference, and match m/z error. Using a chemically modified “decoy” proteome, we demonstrate that these cutoffs reduce the false positive rate with minimal impact on true positives. Elution time filtering provided greater discrimination between true and false positives than mass accuracy, suggesting that further improvements in chromatographic precision will benefit FDR control. We detect a higher estimated FDR compared with previous published models using mixed species (42). However, our analysis differs in two significant aspects: (1) unlike matching between individual “single shot” analyses, our experimental approach assesses match FDR from a fractionated library to a single shot analysis, and (2) unlike a mixed species proteome, our decoy proteome lacks true positives that could prevent assignment to false-positive features. The latter means our reported FDR is likely an overestimate but does provide a metric for assessing the relative FDR when filtering on feature match parameters. In addition, models based on mixed species suggest that matching FDR increases at low sample loads. It will be important in future to assess this with AMPL. In this study, comparable on-column loads between FDR estimation and cell cycle analysis, and therefore, we are confident in the performance of false-positive removal in the cell cycle dataset.

We identify novel proteins whose cell cycle function has not been previously characterized. FAM111B is a PsP in cluster 1 (Fisher's $p_1 < 0.001$, $p_2 = 0.06$), showing peak levels in S-phase populations, followed by a decrease in G2 populations. FAM111B is poorly characterized despite its expression being associated with poor prognosis in pancreatic and liver cancers (Human Protein Atlas (43)) and mutation causative for a rare inherited genetic syndrome (hereditary fibrosing poikiloderma with tendon contracture, myopathy, and pulmonary fibrosis). FAM111A, the only other member of the FAM111 gene family, localizes to newly synthesized chromatin during S phase, interacts with proliferating cell nuclear antigen (PCNA) *via* its PCNA-interacting protein box, and its depletion reduces base incorporation during DNA replication (44). FAM111B also contains a PCNA-interacting

protein box (residues 607–616). Data from HeLa S3 cells also suggest that FAM111B is a cell cycle-regulated protein with peak levels in S phase (45). FAM111B contains D-box and KEN-box motifs that are recognized by the APC/C E3 ligase to ubiquitinate targets for proteasomal degradation. Because of the similarity with FAM111A in sequence, predicted interactions with PCNA, and peak protein abundance in S phase, we propose that FAM111B also is likely to play a key role in DNA replication.

We present an unbiased pseudotemporal analysis of protein abundance changes across eight biochemically resolved mitotic states with a resolution extremely challenging to obtain with high precision using arrest and release methodologies. The frequency of PsPs identified (1.7%; 119/6899) compares well with a recent antibody-based screen for cell cycle-regulated proteins (2.6%; 331/12,390) (46). Included in 331 hits are proteins that vary in subcellular localization but not abundance across the cell cycle, consistent with other datasets using biochemical fractionation (47). PsPs identified in this study will be limited to proteins that change in abundance. However, these PsPs are critical for robust cell state classification of proteomes obtained by MS, most of which do not involve subcellular fractionation.

A high proportion of proteins in clusters 4 and 5 (24/69; 35%) are experimentally validated APC/C substrates, which represents a 70-fold overrepresentation in these two clusters compared with nonpseudoperiodic proteins (0.5%). The high mitotic phase resolution and purity obtained in this study enabled characterization of protein abundance variation of APC/C substrates in mitosis. We identify two waves of mitotic degradation, one coinciding with the destruction of cyclins A and B (cluster 4) and the second at mitotic exit (cluster 5). The unbiased clustering failed to separate cyclin A and cyclin B, which are degraded in prometaphase and at the metaphase-to-anaphase transition, respectively. This can be explained by the relatively few proteins detected that correlate with cyclin A and is consistent with the idea that prometaphase degradation by the APC/C is highly selective. About 44 proteins in clusters 4 and 5 have not been previously experimentally validated as APC/C substrates (29) and are candidates for future follow-up analysis as novel and uncharacterized substrates. These include proteins (e.g., PRC1, KIF23, KIF20A) that were not identified as APC/C-Cdh1 and APC/C-Cdc20 substrates by bioinformatics analysis of coregulation (48) and by chemical biology approaches (49, 50).

High-resolution classification of CCS is an important prerequisite to obtaining meaningful biological insights into single-cell “omics” data. However, datasets on the cell cycle-regulated transcriptome and proteome generally provide low-time resolution, particularly in mitosis. Mitotic time resolution will be crucial for interpreting single-cell proteomes. Whereas transcriptional and translational activity are dampened during mitosis, there are major changes in protein phosphorylation

and protein abundance, which will contribute toward single-cell proteome variation.

Here, we have identified a robust cell cycle signature composed of the abundances from 119 PsPs that can be used to classify the CCS of a cell population by virtue of its cellular proteome. We apply this signature to assign CCSs to hundreds of published proteomic datasets that range in cell type and experimental condition. We have not tested if this signature can be used to assign proteomes from species other than human. We note that many of these proteins are well conserved, with several conserved to yeast (*e.g.*, cyclin, REC8, aurora kinase, polo kinase). We anticipate that this high-resolution cell cycle signature here will be important to understand the biological implications of emerging single-cell proteomics datasets (9, 10), particularly in systems where cell cycle phase differences are an underlying source of variation, as is frequently the case.

Formaldehyde fixation is used frequently as a precursor to intracellular immunostaining for cellular analysis and for inactivating cells that potentially harbor infectious agents, for example, viruses. We have shown that mild formaldehyde treatment is compatible with comprehensive and quantitative proteomics with low cell numbers. We anticipate that the in-cell digest will be broadly applicable to characterize the proteomes of formaldehyde fixed and virally infected cells. Recently published data suggest that formaldehyde crosslinks can be directly detected from MS data (51). We anticipate the in-cell digest would enhance the sensitivity of crosslink detection and lead to an increase in identified protein–protein interactions. The rarest target population are cells in late anaphase of mitosis, which are present in 0.01% of an asynchronous TK6 culture.

DATA AVAILABILITY

Raw MS data and processed MaxQuant output files are available on ProteomeXchange/PRIDE. These data can be accessed using the project accession number PXD028117.

Supplemental data—This article contains [supplemental data](#).

Acknowledgments—The work was supported by the Wellcome Centre for Cell Biology (WCB) core facilities (Wellcome Trust 203149), and funding for instrumentation, including equipment grants to the WCB Proteomics Core (091020) and the flow facilities. We thank for the valuable feedback and discussions with colleagues in the WCB and the University of Edinburgh, including Fiona Rossi (Scottish Centre for Regenerative Medicine), Christos Spanos (WCB), and Shaun Webb (WCB).

Funding and additional information—This work was supported by a Sir Henry Dale Fellowship to T. L. (Wellcome Trust

& Royal Society [206211/Z/17/Z]), a Darwin Trust PhD Studentship to A. A., an EASTBIO PhD Studentship to D. L., and a Medical Research Council Career Development Award to G. K.

Author contributions—V. K. and T. L. conceptualization; V. K., G. K., and T. L. methodology; V. K., G. K., and T. L. formal analysis; V. K., A. A., D. L., and G. K. investigation; G. K. data curation; V. K., G. K., and T. L. writing—original draft; V. K., G. K., and T. L. writing—review and editing; T. L. visualization; T. L. supervision.

Conflict of interest—The authors declare no competing interests.

Abbreviations—The abbreviations used are: AMPL, averaged MS1 precursor library matching; APC/C, anaphase-promoting complex/cyclosome; BSA, bovine serum albumin; CCS, cell cycle state; DDA, data-dependent acquisition; DPBS, Dulbecco's PBS; FACS, fluorescence-activated cell sorting; FDR, false discovery rate; HPRP, high pH reversed-phase; LCL, lymphoblastoid cell line; MBR, match-between-runs; NCC, nascent chromatin capture; NES, nuclear export signal; PCA, principal component analysis; PCNA, proliferating cell nuclear antigen; PRIMMUS, PRoteomics of Intra-cellular IMMUnostained cell Subsets; PsP, pseudoperiodic protein; RO, RO-3306; S/N, signal-to-noise; SILAC, stable isotope labeling by amino acids in cell culture; SLiM, short linear (sequence) motif; WCB, Wellcome Centre for Cell Biology.

Received April 20, 2021, and in revised form, September 2, 2021
Published, MCPRO Papers in Press, November 4, 2021, <https://doi.org/10.1016/j.mcpro.2021.100169>

REFERENCES

1. Ly, T., Whigham, A., Clarke, R., Brenes-Murillo, A. J., Estes, B., Madhessian, D., Lundberg, E., Wadsworth, P., and Lamond, A. I. (2017) Proteomic analysis of cell cycle progression in asynchronous cultures, including mitotic subphases, using PRIMMUS. *Elife* **6**, e27574
2. Ly, T., Endo, A., and Lamond, A. I. (2015) Proteomic analysis of the response to cell cycle arrests in human myeloid leukemia cells. *Elife* **4**, e04534
3. [preprint] Ly, T., Whigham, A., Clarke, R., Brenes-Murillo, A. J., Estes, B., Wadsworth, P., and Lamond, A. I. (2017) Proteomic analysis of cell cycle progression in asynchronous cultures, including mitotic subphases, using PRIMMUS. *bioRxiv*. <https://doi.org/10.1101/125831>
4. Kelly, R. T. (2020) Single-cell proteomics: Progress and prospects. *Mol. Cell. Proteomics* **19**, 1739–1748
5. Specht, H., Emmott, E., Petelski, A. A., Huffman, R. G., Periman, D. H., Serra, M., Kharchenko, P., Koller, A., and Slavov, N. (2021) Single-cell proteomic and transcriptomic analysis of macrophage heterogeneity using SCoPE2. *Genome Biol.* **22**, 50
6. Wiśniewski, J. R., Zougman, A., Nagaraj, N., and Mann, M. (2009) Universal sample preparation method for proteome analysis. *Nat. Methods* **6**, 359–362
7. Hughes, C. S., Foehr, S., Garfield, D. A., Furlong, E. E., Steinmetz, L. M., and Krijgsveld, J. (2014) Ultrasensitive proteome analysis using paramagnetic bead technology. *Mol. Syst. Biol.* **10**, 757
8. Zhang, Z., Dubiak, K. M., Huber, P. W., and Dovichi, N. J. (2020) Miniaturized filter-aided sample preparation (MICRO-FASP) method for high

- throughput, ultrasensitive proteomics sample preparation reveals proteome asymmetry in *Xenopus laevis* embryos. *Anal. Chem.* **92**, 5554–5560
9. [preprint] Brunner, A.-D., Thielert, M., Vasilopoulou, C. G., Ammar, C., Coscia, F., Mund, A., Hoerning, O. B., Bache, N., Apalategui, A., Lubeck, M., Richter, S., Fischer, D. S., Raether, O., Park, M. A., Meier, F., et al. (2021) Ultra-high sensitivity mass spectrometry quantifies single-cell proteome changes upon perturbation. *bioRxiv*. <https://doi.org/10.1101/2020.12.22.423933>
 10. [preprint] Hartlmayr, D., Ctorteccka, C., Seth, A., Mendjan, S., Toumiaire, G., and Mechtler, K. (2021) An automated workflow for label-free and multiplexed single cell proteomics sample preparation at unprecedented sensitivity. *bioRxiv*. <https://doi.org/10.1101/2021.04.14.439828>
 11. Zhu, Y., Piehowski, P. D., Zhao, R., Chen, J., Shen, Y., Moore, R. J., Shukla, A. K., Petyuk, V. A., Campbell-Thompson, M., Mathews, C. E., Smith, R. D., Qian, W.-J., and Kelly, R. T. (2018) Nanodroplet processing platform for deep and quantitative proteome profiling of 10–100 mammalian cells. *Nat. Commun.* **9**, 882
 12. Metz, B., Kersten, G. F. A., Hoogerhout, P., Brugghe, H. F., Timmermans, H. A. M., de Jong, A., Meiring, H., ten Hove, J., Hennink, W. E., Crommelin, D. J., and Jiskoot, W. (2004) Identification of formaldehyde-induced modifications in proteins: Reactions with model peptides. *J. Biol. Chem.* **279**, 6235–6243
 13. Toews, J., Rogalski, J. C., Clark, T. J., and Kast, J. (2008) Mass spectrometric identification of formaldehyde-induced peptide modifications under *in vivo* protein cross-linking conditions. *Anal. Chim. Acta* **618**, 168–183
 14. Skopek, T. R., Liber, H. L., Penman, B. W., and Thilly, W. G. (1978) Isolation of a human lymphoblastoid line heterozygous at the thymidine kinase locus: Possibility for a rapid human cell mutation assay. *Biochem. Biophys. Res. Commun.* **84**, 411–416
 15. Cox, J., and Mann, M. (2008) MaxQuant enables high peptide identification rates, individualized p.p.b.-range mass accuracies and proteome-wide protein quantification. *Nat. Biotechnol.* **26**, 1367–1372
 16. Mohammed, H., Taylor, C., Brown, G. D., Papachristou, E. K., Carroll, J. S., and D'Santos, C. S. (2016) Rapid immunoprecipitation mass spectrometry of endogenous proteins (RIME) for analysis of chromatin complexes. *Nat. Protoc.* **11**, 316–326
 17. Tyanova, S., Temu, T., and Cox, J. (2016) The MaxQuant computational platform for mass spectrometry-based shotgun proteomics. *Nat. Protoc.* **11**, 2301–2319
 18. Pasa-Tolić, L., Masselon, C., Barry, R. C., Shen, Y., and Smith, R. D. (2004) Proteomic analyses using an accurate mass and time tag strategy. *Bio-techniques* **37**, 621–639
 19. Meier, F., Geyer, P. E., Virreira Winter, S., Cox, J., and Mann, M. (2018) BoxCar acquisition method enables single-shot proteomics at a depth of 10,000 proteins in 100 minutes. *Nat. Methods* **15**, 440–448
 20. Clute, P., and Pines, J. (1999) Temporal and spatial control of cyclin B1 destruction in metaphase. *Nat. Cell Biol.* **1**, 82–87
 21. Elzen den, N., and Pines, J. (2001) Cyclin a is destroyed in prometaphase and can delay chromosome alignment and anaphase. *J. Cell Biol.* **153**, 121–136
 22. Koo, S. J., Fernández-Montalván, A. E., Badock, V., Ott, C. J., Holton, S. J., von Ahlsen, O., Toedling, J., Vittori, S., Bradner, J. E., and Gorjánác, M. (2016) ATAD2 is an epigenetic reader of newly synthesized histone marks during DNA replication. *Oncotarget* **7**, 70323–70335
 23. Kumar, M., Gouw, M., Michael, S., Sámano-Sánchez, H., Pancsa, R., Glavina, J., Diakogianni, A., Valverde, J. A., Bukirova, D., Čalyševa, J., Palopoli, N., Davey, N. E., Chemes, L. B., and Gibson, T. J. (2019) ELM—the eukaryotic linear motif resource in 2020. *Nucleic Acids Res.* **48**, D296–D306
 24. Gonçalves, V., and Jordan, P. (2015) Posttranscriptional regulation of splicing factor SRSF1 and its role in cancer cell biology. *Biomed. Res. Int.* **2015**, 287048
 25. Breig, O., and Baklouti, F. (2013) Proteasome-mediated proteolysis of SRSF5 splicing factor intriguingly co-occurs with SRSF5 mRNA upregulation during late erythroid differentiation. *PLoS One* **8**, e59137
 26. Maréchal, A., and Zou, L. (2013) DNA damage sensing by the ATM and ATR kinases. *Cold Spring Harb. Perspect. Biol.* **5**, a012716
 27. Kernan, J., Bonacci, T., and Emanuele, M. J. (2018) Who guards the guardian? Mechanisms that restrain APC/C during the cell cycle. *Biochim. Biophys. Acta Mol. Cell Res.* **1865**, 1924–1933
 28. Chang, L., and Barford, D. (2014) Insights into the anaphase-promoting complex: A molecular machine that regulates mitosis. *Curr. Opin. Struct. Biol.* **29**, 1–9
 29. Davey, N. E., and Morgan, D. O. (2016) Building a regulatory network with short linear sequence motifs: Lessons from the degrons of the anaphase-promoting complex. *Mol. Cell* **64**, 12–23
 30. Di Fiore, B., Davey, N. E., Hagting, A., Izawa, D., Mansfeld, J., Gibson, T. J., and Pines, J. (2015) The ABBA motif binds APC/C activators and is shared by APC/C substrates and regulators. *Dev. Cell* **32**, 358–372
 31. Lara-Gonzalez, P., Scott, M. I. F., Diez, M., Sen, O., and Taylor, S. S. (2011) BubR1 blocks substrate recruitment to the APC/C in a KEN-box-dependent manner. *J. Cell Sci.* **124**, 4332–4345
 32. Hellmuth, S., Gómez-H, L., Pendás, A. M., and Stemmann, O. (2020) Securin-independent regulation of separase by checkpoint-induced shugoshin-MAD2. *Nature* **580**, 536–541
 33. Stegle, O., Teichmann, S. A., and Marioni, J. C. (2015) Computational and analytical challenges in single-cell transcriptomics. *Nat. Rev. Genet.* **16**, 133–145
 34. Scialdone, A., Natarajan, K. N., Saraiva, L. R., Proserpio, V., Teichmann, S. A., Stegle, O., Marioni, J. C., and Buettner, F. (2015) Computational assignment of cell-cycle stage from single-cell transcriptome data. *Methods* **85**, 54–61
 35. Liu, Z., Lou, H., Xie, K., Wang, H., Chen, N., Aparicio, O. M., Zhang, M. Q., Jiang, R., and Chen, T. (2017) Reconstructing cell cycle pseudo time-series via single-cell transcriptome data. *Nat. Commun.* **8**, 22
 36. Cuomo, A. S. E., Seaton, D. D., McCarthy, D. J., Martinez, I., Bonder, M. J., Garcia-Bernardo, J., Amatya, S., Madrigal, P., Isaacson, A., Buettner, F., Knights, A., Natarajan, K. N., HipSci Consortium, Vallier, L., Marioni, J. C., et al. (2020) Single-cell RNA-sequencing of differentiating iPSCs reveals dynamic genetic effects on gene expression. *Nat. Commun.* **11**, 810
 37. Ly, T., Ahmad, Y., Shlien, A., Soroka, D., Mills, A., Emanuele, M. J., Stratton, M. R., and Lamond, A. I. (2014) A proteomic chronology of gene expression through the cell cycle in human myeloid leukemia cells. *Elife* **3**, e01630
 38. Kustatscher, G., Grabowski, P., Schrader, T. A., Passmore, J. B., Schrader, M., and Rappsilber, J. (2019) Co-regulation map of the human proteome enables identification of protein functions. *Nat. Biotechnol.* **37**, 1361–1371
 39. Fierro-Monti, I., Echeverria, P., Racle, J., Hernandez, C., Picard, D., and Quadroni, M. (2013) Dynamic impacts of the inhibition of the molecular chaperone Hsp90 on the T-cell proteome have implications for anti-cancer therapy. *PLoS One* **8**, e80425
 40. Bath, T. S., Tollenaere, M. X., Rütger, P., Gonzalez-Franquesa, A., Prabhakar, B. S., Bekker-Jensen, S., Deshmukh, A. S., and Olsen, J. V. (2019) Protein aggregation capture on microparticles enables multipurpose proteomics sample preparation. *Mol. Cell. Proteomics* **18**, 1027–1035
 41. Yu, F., Haynes, S. E., and Nesvizhskii, A. I. (2021) IonQuant enables accurate and sensitive label-free quantification with FDR-controlled match-between-runs. *Mol. Cell. Proteomics* **20**, 100077
 42. Tsai, C. F., Zhao, R., Williams, S. M., Moore, R. J., Schultz, K., Chrisler, W. B., Pasa-Tolic, L., Rodland, K. D., Smith, R. D., Shi, T., Zhu, Y., and Liu, T. (2020) An improved boosting to amplify signal with isobaric labeling (iBASIL) strategy for precise quantitative single-cell proteomics. *Mol. Cell. Proteomics* **19**, 828–838
 43. Uhlen, M., Zhang, C., Lee, S., Sjöstedt, E., Fagerberg, L., Bidkhor, G., Benfiteas, R., Arif, M., Liu, Z., Edfors, F., Sanli, K., von Feilitzen, K., Oksvold, P., Lundberg, E., Hober, S., et al. (2017) A pathology atlas of the human cancer transcriptome. *Science* **357**, eaan2507
 44. Alabert, C., Bukowski-Wills, J. C., Lee, S. B., Kustatscher, G., Nakamura, K., de Lima Alves, F., Menard, P., Mejlvang, J., Rappsilber, J., and Groth, A. (2014) Nascent chromatin capture proteomics determines chromatin dynamics during DNA replication and identifies unknown fork components. *Nat. Cell Biol.* **16**, 281–291
 45. Aviner, R., Shenoy, A., Elroy-Stein, O., and Geiger, T. (2015) Uncovering hidden layers of cell cycle regulation through integrative multi-omic analysis. *PLoS Genet.* **11**, e1005554
 46. Mahdessian, D., Cesnik, A. J., Gnann, C., Danielsson, F., Stenström, L., Arif, M., Zhang, C., Le, T., Johansson, F., Shutten, R., Bäckström, A., Axelsson, U., Thul, P., Cho, N. H., Carja, O., et al. (2021) Spatiotemporal dissection of the cell cycle with single-cell proteogenomics. *Nature* **590**, 649–654
 47. Herr, P., Boström, J., Rullman, E., Rudd, S. G., Vesterlund, M., Lehtiö, J., Helleday, T., Maddalo, G., and Altun, M. (2020) Cell cycle profiling reveals protein oscillation, phosphorylation, and localization dynamics. *Mol. Cell. Proteomics* **19**, 608–623

48. Franks, J. L., Martinez-Chacin, R. C., Wang, X., Tiedemann, R. L., Bonacci, T., Choudhury, R., Bolhuis, D. L., Enrico, T. P., Mouery, R. D., Damrauer, J. S., Yan, F., Harrison, J. S., Major, M. B., Hoadley, K. A., Suzuki, A., *et al.* (2020) In silico APC/C substrate discovery reveals cell cycle-dependent degradation of UHRF1 and other chromatin regulators. *PLoS Biol.* **18**, e3000975
49. Bakos, G., Yu, L., Gak, I. A., Roumeliotis, T. I., Liakopoulos, D., Choudhary, J. S., and Mansfeld, J. (2018) An E2-ubiquitin thioester-driven approach to identify substrates modified with ubiquitin and ubiquitin-like molecules. *Nat. Commun.* **9**, 4776
50. Manohar, S., Yu, Q., Gygi, S. P., and King, R. W. (2020) The insulin receptor adaptor IRS2 is an APC/C substrate that promotes cell cycle protein expression and a robust spindle assembly checkpoint. *Mol. Cell. Proteomics* **19**, 1450–1467
51. Tayri-Wilk, T., Slavin, M., Zamel, J., Blass, A., Cohen, S., Motzik, A., Sun, X., Shalev, D. E., Ram, O., and Kalisman, N. (2020) Mass spectrometry reveals the chemistry of formaldehyde cross-linking in structured proteins. *Nat. Commun.* **11**, 3128